Analysis of a quantum logic device based on dipole-dipole interactions of optically trapped Rydberg atoms

M. Saffman and T. G. Walker
Department of Physics, University of Wisconsin, 1150 University Avenue, Madison, Wisconsin 53706, USA
(Received 8 February 2005; published 31 August 2005)

We present a detailed analysis and design of a neutral atom quantum logic device based on atoms in optical traps interacting via dipole-dipole coupling of Rydberg states. The dominant physical mechanisms leading to decoherence and loss of fidelity are enumerated. Our results support the feasibility of performing single- and two-qubit gates at MHz rates with decoherence probability and fidelity errors at the level of 10^{-3} for each operation. Current limitations and possible approaches to further improvement of the device are discussed.

DOI: 10.1103/PhysRevA.72.022347 PACS number(s): 03.67.Lx, 32.80.Qk

I. INTRODUCTION

Motivated by the discovery that quantum algorithms can provide exponential gains for solving certain computational problems, numerous proposals have been advanced for experimental realization of a quantum computer [1]. While a useful processor remains far off, ground breaking experiments have demonstrated controlled evolution of a few qubits and implemented basic quantum algorithms for computation and error correction [2–8]. Among the range of physical systems that have been identified as candidates for implementing quantum logic the most extensive laboratory results so far have been obtained with cold trapped ions [9] and nuclear magnetic resonance (NMR) in macroscopic samples [10,11].

Within the last few years neutral atoms have emerged as a possible route to experimental quantum logic. The most obvious distinguishing feature between neutral atom and trapped ion schemes is the absence of strong Coulomb forces in the former. Coulomb forces between ions couple strongly the motional degrees of freedom. This can be utilized to entangle any two of a linear string of ions, as was first elucidated in the work of Cirac and Zoller [12] and demonstrated experimentally in Boulder [13] and Innsbruck [14]. The lack of a strong Coulomb interaction in neutral atoms is advantageous as regards decoherence, since coupling to stray fields is weaker for atoms than for ions. The drawback, and indeed the central difficulty in constructing a large scale quantum processor, is the need for strong qubit to qubit coupling, while maintaining weak coupling to the environment. Neutral atom coupling based on ground-state collisions, light mediated dipole-dipole coupling, and dipole-dipole coupling of highly excited Rydberg states have all been proposed in the last several years [15–20]. In particular dipole-dipole coupling of Rydberg states provides a strong interaction suitable for the implementation of fast gates [21], and this paper is devoted to a detailed study of this approach.

While the theoretical foundations of the Jaksch *et al.* Rydberg state dipole-dipole coupling approach to quantum logic have been presented [21], the question of how to implement this scheme in a practical and scalable fashion has not been solved [22]. Regardless of how logical operations are to be performed, there are two primary obstacles that must be surmounted. The first is how to create a large number of trapping sites, and load a single atom into each site. This amounts to initialization of the quantum computer. The second difficulty is that in order to be useful for generic models of quantum computation the sites must be individually accessible for logical operations, and state readout. In this paper we do not discuss the problem of creation and loading of a large number of addressable single atom sites. A number of possible solutions to these questions have been discussed in the literature [23–30].

Our goal here is to examine in detail the use of two closely spaced sites, each containing a neutral atom qubit, for high fidelity quantum operations. Far-off-resonance optical traps (FORTs) are defined by tightly focusing laser light in a set of chosen locations. Single atoms are loaded into the optical traps after precooling in a magneto-optical trap [31,32]. Single-qubit operations are performed using two-photon stimulated Raman transitions, and a two-qubit conditional phase gate is realized using dipole-dipole coupling of atoms excited to high lying Rydberg states [21]. Qubit measurement is performed by counting resonance fluorescence photons.

The ability to perform many operations with high fidelity and low decoherence is a prerequisite for scaling up to a larger number of qubits. As will be shown in what follows, our calculations lead to the conclusion that a set of logically complete qubit operations can be performed with high fidelity at MHz rates. This would suggest that qubit storage in optical traps with coherence times of much less than a second will be sufficient for large computations. However, the necessity of implementing error correction implies that a computation will also require a large number of state measurements, which are projected to be several orders of magnitude slower than the logical operations. We therefore examine closely the feasibility of T_1 and T_2 coherence times of several seconds in optical traps.

The remainder of this paper is structured as follows. In Sec. II we estimate the decoherence times for storage of individual atoms in FORTs. We specifically include the contributions due to collisions with hot background atoms (Sec. II B), photon scattering from the trapping laser (Sec. II C), spin flips due to the trapping laser, and heating rates due to laser noise (Sec. II D). Decoherence due to fluctuations in the

trapping lasers is considered in Sec. II E and due to background fields in Sec. II F.

In Sec. III we discuss the operation of single-qubit gates based on two-photon stimulated Raman transitions. In particular we calculate decoherence probabilities due to excited-state spontaneous emission (Sec. III A) and expected gate fidelities due to ac Stark shifts (Sec. III B) and motional effects (Sec. III C). Leakage out of the computational basis due to imperfect optical polarization is estimated in Sec. III D and limitations imposed by the laser stability are estimated in Sec. III E. The ability to rapidly interrogate the atomic state is crucial to the usefulness of this approach. We discuss single atom state detection using collection of resonance fluorescence in Sec. III F. Included in Sec. III F is a discussion of heating during readout, and its amelioration using red-detuned molasses for the interrogation beams.

In Sec. IV we discuss the implementation of a two-qubit conditional phase gate which can serve as a logical primitive for arbitrary computations. We consider two different regimes of operation: Rabi frequency large compared to dipole-dipole frequency shift (Sec. IV A) and dipole-dipole frequency shift large compared to Rabi frequency (Sec. IV B).

Two-qubit operations involving Rydberg states have larger errors and higher decoherence rates than single-qubit operations. We optimize the parameters of a phase gate in the two limits of weak dipole-dipole interaction (Sec. IV A) and strong dipole-dipole interaction (Sec. IV B). In both cases the performance depends critically on the Rydberg state lifetime which we calculate for relevant experimental parameters in Secs. IV E and IV F. An additional aspect of the Rydberg state interactions that needs to be addressed is the rate of heating due to differences in the ground-state and excited-state polarizabilities. We show how to minimize this effect at the expense of some additional decoherence in Sec. IV D.

The results of the calculations of fidelities and decoherence rates provide a picture of the feasibility of a quantum logic device capable of executing a large number of sequential gate operations. We discuss the expected overall performance of this approach to quantum computing in Sec. V, and highlight the areas that are most troublesome. Possible extensions to the techniques discussed here that have the potential for improved performance are discussed.

II. OPTICAL TRAPS FOR SINGLE ATOMS

In this section we recall some basic features of far off resonant optical traps. A number of distinct physical mechanisms limit the coherence of atoms stored in FORTs. Some of these decohering effects are intrinsic to the operation of the FORT, and some are due to technical imperfections of the apparatus used. As shown in Table I these mechanisms contribute to an effective decoherence time of diagonal (T_1) or off-diagonal (T_2) density-matrix elements. We discuss the physics behind each of these decohering mechanisms in the following subsections. All numerical estimates of decoherence rates will be calculated for ^{87}Rb atoms using the parameters listed in Table I.

TABLE I. Physical mechanisms limiting ground-state coherence of qubit basis states $|a\rangle=|F=1,m_F=0\rangle$ and $|b\rangle=|F=2,m_F=0\rangle$. Values listed are for $P=1\times10^{-10}$ mbar, $U_m=1$ mK, $T_a=50$ μK, $\lambda_f=1.01$ μm, and $w_{f0}=2.5$ μm, and $\alpha_0(\omega_f)=114$ Å^3. See text for details and additional parameters.

Mechanism	Section	T_1 (sec)	T_2 (sec)
Background gas collisions	II B	55	
Rayleigh scattering	II C	97	
Raman scattering	II C	151	
Laser noise heating	II D	20	
ac stark shifts, intensity noise	II E		12
ac stark shifts, motional	II E		2.6
Background B field	II F		56
Combined		12	2.1

A. FORT trap parameters

In its simplest form an optical FORT trap can be created by focusing a single laser beam of wavelength λ_f to a waist w_{f0} [33,34]. The ground-state ac Stark shift due to a far-detuned trapping beam is

$$U_{\rm ac}=-\frac{1}{4}|\mathcal{E}_f|^2\boldsymbol{\epsilon}^*\cdot\langle i|\hat{\boldsymbol{\alpha}}|i\rangle\cdot\boldsymbol{\epsilon}, \tag{1}$$

where $\mathcal{E}_f$ is the amplitude of the optical field, the laser intensity is $I_f=\epsilon_0 c|\mathcal{E}_f|^2/2$, and $\boldsymbol{\epsilon}$ is the trapping laser polarization. The polarizability is in general the sum of scalar, vector, and tensor parts [35]. For a $J=1/2$ ground state with a linearly polarized trapping beam we need only consider the scalar polarizability which we calculate numerically using Coulomb wave functions to be $\alpha_0=114$ Å^3 for a trapping laser at $\lambda_f=1.01$ μm.

The maximum depth of the potential well at the center of the focused beam expressed in temperature units is $U_m=-\alpha_0|\mathcal{E}_f|^2/4$. The spatial dependence of the trapping potential is then

$$U_f(x,y,z)=U_m\frac{e^{-2(x^2+y^2)/w_f^2(z)}}{1+\dfrac{z^2}{L_f^2}}, \tag{2}$$

where for a FORT beam propagating along z, $w_f^2(z)=w_{f0}^2(1+z^2/L_f^2)$, with the Rayleigh length $L_f=\pi w_{f0}^2/\lambda_f$. For the parameters of Table I a laser power of 60 mW gives $U_m=1$ mK.

The FORT can be directly loaded from a Magneto-optical trap (MOT) provided that the product of the capture volume and the MOT density is larger than unity. A first approximation for the capture volume assumes that all atoms in the region where $|U_f/k_B|>T_c$ are captured, while those outside this region are lost (in the rest of the paper we will express all energies in temperature units and put $k_B=1$). We expect that the capture temperature T_c will be similar to T_a, the kinetic temperature of the atoms in the MOT, provided T_a is smaller than $|U_m|$. We define a relative trap depth χ

$=|U_m|/T_a$, so that the capture volume vanishes for $\chi=1$, and increases monotonically with increasing χ. A simple calculation then results in an expression for the capture volume,

$$V = 2\int_0^{z_m} dz\ \pi r_m^2(z) = \pi w_{f0}^2 \int_0^{z_m} dz \left(1+\frac{z^2}{L_f^2}\right) \ln\left(\frac{z_m^2+L_f^2}{z^2+L_f^2}\right)$$
$$= \frac{4\pi}{3} w_{f0}^2 z_m + \frac{2\pi}{9}\frac{w_{f0}^2}{L_f^2}\left[z_m^3 - 6L_f^3 \tan^{-1}\left(\frac{z_m}{L_f}\right)\right] \quad (3)$$

with $z_m=L_f\sqrt{\chi-1}$. Using numerical values from Table I we get a capture volume of 8.6×10^{-9} cm^3. We have found in unpublished experiments that a MOT density of a few times 10^8/cm^3 is sufficient to load single atoms as was demonstrated by several groups in recent years [31,32].

In the context of quantum logic it is important that the atoms are well localized in position and momentum. We can estimate the variances of the atomic position and momentum by making a parabolic expansion of the FORT potential about the origin. The effective spring constants of the trap are found to be

$$\kappa_x = \kappa_y = 4\frac{|U_m|}{w_{f0}^2}, \quad (4a)$$

$$\kappa_z = 2\frac{|U_m|}{L_f^2} \quad (4b)$$

and the corresponding oscillation frequencies are

$$\omega_x = \omega_y = \frac{2}{w_{f0}}\left(\frac{|U_m|}{m}\right)^{1/2}, \quad (5a)$$

$$\omega_z = \frac{\sqrt{2}}{L_f}\left(\frac{|U_m|}{m}\right)^{1/2}, \quad (5b)$$

with m the atomic mass. For the above parameters and ^{87}Rb we find $\omega_{(x,z)}/(2\pi)=(39,3.6)$ kHz. At $T_a=50$ μK many vibrational levels will be excited and we can use Boltzmann factors to estimate the time averaged variances of the position and momentum as

$$\langle x_a^2\rangle = \langle y_a^2\rangle = \frac{w_{f0}^2}{4}\frac{T_a}{|U_m|}, \quad (6a)$$

$$\langle z_a^2\rangle = \frac{\pi^2 w_{f0}^4}{2\lambda_f^2}\frac{T_a}{|U_m|}, \quad (6b)$$

$$\langle v_{xa}^2\rangle = \langle v_{ya}^2\rangle = \langle v_{za}^2\rangle = \frac{T_a}{m}. \quad (6c)$$

Note that the spatial localization along z can be written in terms of an anisotropy factor $\xi_f=\sqrt{\kappa_x/\kappa_z}=\sqrt{2}\pi w_{f0}/\lambda_f$ such that $\langle z_a^2\rangle=\xi_f^2\langle x_a^2\rangle$.

B. Background gas collisions

Collisions with untrapped background atoms in the vacuum chamber result in heating and loss of atoms from the FORT and therefore limit the storage time and T_1 that can be achieved. The characteristic energy change for which diffractive collisions must be accounted for is $\sim$2.8 mK for Rb [36]. As we are considering a shallow FORT of depth $|U_m|=1$ mK we will neglect diffractive and heating effects and approximate the FORT lifetime due to background collisions mediated by a van der Waals interaction as [36]

$$\frac{1}{\tau_c} = \sqrt{\frac{3T_b}{m}} n_b \sigma_{\text{Rb-Rb}} \quad (7)$$

with $T_b=300$ K the temperature of the thermal background atoms of density n_b. Using $\sigma_{\text{Rb-Rb}}=2.5\times10^{-13}$ cm^2 [36] we find $\tau_c=55$ s at a pressure of 1×10^{-10} mbar. Even without resorting to cryogenic vacuum systems pressures as low as 10^{-11} mbar are achievable, which would imply collisional lifetimes of order 10 min. These estimates are consistent with observations [31] of FORT decay times using Cs atoms of 50 sec at pressures of about 10^{-10} mbar.

C. Photon scattering

Scattering of FORT light by the qubit atoms causes some heating and leads to a small amount of decoherence. The scattering can be separated into two contributions. Elastic or Rayleigh scattering of the FORT light does not change or dephase the qubit spin but does heat the external degrees of freedom of the atoms. Inelastic or Raman scattering occurs at a much reduced rate but, since it changes the spin state of the qubit atom it does contribute to decoherence, albeit at a small rate.

The elastic scattering cross section is

$$\sigma_e = \frac{8\pi}{3} k_f^4 |\alpha_0|^2 = 1.6\times10^{-24}\ \text{cm}^2, \quad (8)$$

where $k_f=2\pi/\lambda_f$. To get the numerical value we have used the parameters given in Table I. This scattering produces a heating rate

$$\frac{dE}{dt} = \frac{\hbar^2 k_f^2}{2m}\frac{\sigma_e I_f}{\hbar\omega_f} = \frac{\hbar\omega_f \sigma_e I_f}{2mc^2}. \quad (9)$$

Since both the heating rate and the trap depth U scale with intensity, their ratio gives the characteristic heating time for an atom in the FORT

$$\frac{|U_m|}{dE/dt} = \frac{2\alpha_0 m\lambda_f}{\hbar\sigma_e} = 1950\ \text{s}. \quad (10)$$

A more conservative definition of the T_1 due to Rayleigh scattering is the time for the atom to double its motional energy, which gives $T_1=97$ s for the parameters of Table I.

The inelastic scattering cross section can be expressed in terms of the vector polarizability α_1 as

$$\sigma_{\text{ie}} = \frac{4\pi}{3} k^4 |\alpha_1|^2 = 2.3\times10^{-27}\ \text{cm}^2, \quad (11)$$

where we have used $\alpha_1\approx-6$ Å^3. The smallness of the inelastic cross section comes from the small coupling of the FORT light to the electron spin of the atom which scales with the

ratio of the fine-structure splitting of the Rb P levels to the detuning of the FORT laser.

Since the inelastic scattering destroys the qubit state, it is a source of decoherence. It is proportional to FORT intensity, so it can be reduced if necessary by operating at low trap depths. The qubit longitudinal relaxation time due to inelastic scattering is

$$T1_{\mathrm{ie}} = \frac{1}{\sigma_{\mathrm{ie}} I_f/(\hbar\omega_f)} = \frac{3\hbar\lambda_f^3|\alpha_0|}{16\pi^3|U_m|\alpha_1^2} = \frac{1}{|U_m|\ (\mathrm{mK})} \times 151\ \mathrm{s}, \tag{12}$$

which is very long even for a robust 1-mK trap depth.

D. Laser noise induced heating

Laser intensity and pointing fluctuations can cause undesirable heating in FORTs [37]. The heating rate due to intensity noise is

$$\frac{dT_a}{dt} = \pi^2\nu^2 S_i(2\nu) T_a, \tag{13}$$

where ν is the trap oscillation frequency, and $S_i(2\nu)$ is the one-sided power spectrum of the fractional intensity fluctuations. These fluctuations are usually far above the shot-noise limit $S_i = 2h\nu/P = 4\times10^{-18}/\mathrm{Hz}$ at the 1–100-kHz frequencies of interest here. As indicated above a 1-mK FORT depth requires 60 mW of $\lambda_f = 1.01$-μm laser power which can be readily supplied by a small diode laser. A typical fluctuation level for an unstabilized diode laser is $S_i = 10^{-12}/\mathrm{Hz}$. The characteristic time for an atom to be heated out of the trap is

$$T_1 = \frac{1}{\pi^2\nu^2 S_i(2\nu)} \ln\left(\frac{|U_m|}{T_a}\right). \tag{14}$$

Using the values given in Table I and $\nu = 39$ kHz gives $T_1 \simeq 50$ s. If necessary, feedback can be used to reduce the laser noise and extend the heating time.

Fluctuations in the laser beam position are also a source of heating. The characteristic heating time can be written as

$$T_1 = \frac{\langle x_a^2\rangle}{\pi^2\nu^2 S_x(\nu)} \ln\left(\frac{|U_m|}{T_a}\right), \tag{15}$$

where S_x is the frequency spectrum of the position fluctuations. The parameters of Table I and Eq. (6a) give $\sqrt{\langle x_a^2\rangle} = 0.28\ \mu$m. To obtain $T_1 = 50$ s requires $\sqrt{S_x} = 5.6\times10^{-7}\ \mu\mathrm{m}/\sqrt{\mathrm{Hz}}$ which is feasible with careful attention to mechanical construction.

Finally for an anisotropic trap there is also heating from beam-steering fluctuations. This implies, for a highly anisotropic trap of aspect ratio ξ_f, a heating time of

$$T_1 = \frac{1}{\pi^2\nu^2\xi_f^2 S_\theta(\nu)} \ln\left(\frac{|U_m|}{T_a}\right), \tag{16}$$

where S_θ is the spectrum of angular fluctuations of the FORT laser beam. For the parameters we are using $\xi_f \sim 8$ so there is a strong sensitivity to beam-steering noise. Nonetheless, it should be feasible using fiber optic delivery of the trapping beam to achieve $T_1 \sim 50$ s.

To summarize this section, estimates of storage times due to technical noise induced heating are of order 50 s, for three different mechanisms. Without appealing to extraordinary technical developments we can set the total contribution due to technical laser noise as $T_1 \sim 20$ s. Ultimately this number could be improved by several orders of magnitude before reaching limits set by quantum fluctuations.

E. ac Stark shifts

In the preceding sections we have discussed decoherence mechanisms that to an excellent approximation affect the qubit ground states equally. Therefore no dephasing of the qubit basis states is incurred and there is no contribution to a finite transverse relaxation time, T_2. As will be discussed in Sec. III we will use the states $|a\rangle = |F=1, m_F=0\rangle$ and $|b\rangle = |F=2, m_F=0\rangle$ as our computational basis. In the absence of any applied fields these states have a hyperfine splitting $U_{\mathrm{hf}}(0)/h \simeq 6.83$ GHz. In the presence of a static electric field there is a correction to the hyperfine splitting in ^{87}Rb given by [38]

$$U_{hf}(E) \simeq U_{\mathrm{hf}}(0)\left\{1 - \alpha_s(0)E^2\left[\frac{1}{2(U_{n=5,L=1} - U_{n=5,L=0})} + \frac{1}{U_{n=4,L=2} - U_{n=5,L=0}}\right]\right\}, \tag{17}$$

where $\alpha_s(0)$ is the static polarizability and E is the electric-field amplitude. For a far detuned trapping laser with a photon energy that is small compared to the term differences that appear in Eq. (17) we can estimate the shift by making the replacement $\alpha_s(0)E^2 \to \alpha_s(\omega_f)|\mathcal{E}|^2/2$ so that Eq. (17) can be written as $U_{hf}(\mathcal{E}) = U_{hf}(0) - \beta U_{\mathrm{ac}}$ where $\beta = 2U_{hf}(0)[\cdots]$, with $[\cdots]$ the term in square brackets in Eq. (17). For ^{87}Rb we find $\beta = 4.1\times10^{-5}$. At a trap depth of $|U_m| = 1$ mK the correction to U_{hf} is $\beta U_{\mathrm{ac}} \simeq 1500$ Hz.

If the trapping laser had no intensity fluctuations and there was no atomic motion this small correction to the hyperfine shift would be time independent and would only give an unimportant correction to the hyperfine splitting. However, intensity noise and atomic motion result in a time-dependent shift which gives a finite T_2. We consider first the effect of intensity noise which results in state dependent dephasing due to fluctuations in $U_{hf}(\mathcal{E})$. When the averaged fluctuation vanishes over the time scale of interest there will be no additional decoherence, and indeed intensity fluctuations are not expected to be problematic for μs time scale gate operations. However, as regards storage of quantum information during a long calculation it is necessary to consider slow drifts in laser intensity that will give qubit dephasing. We define an effective T_2 due to dephasing by

$$T_2 = \frac{2\pi\hbar}{\delta U_{\mathrm{hf}}(\mathcal{E})} = \frac{2\pi\hbar}{\beta U_{ac}} \frac{I}{\delta I}, \tag{18}$$

where $\delta I/I$ is the fractional intensity fluctuation. The relative intensity noise is a function of frequency. In an actively stabilized system the fluctuations will be very small at high frequencies. We are most concerned about finite fluctuations

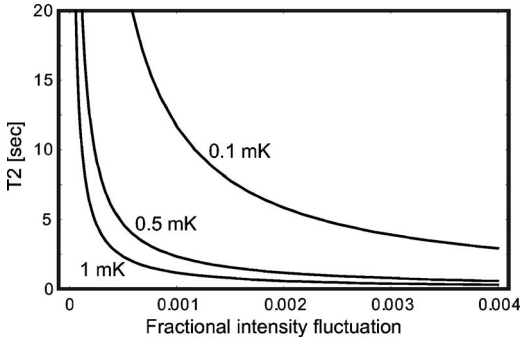

FIG. 1. Effective T_2 due to differential ac stark shift of hyperfine levels for trap depths of 1, 0.5, and 0.1 mK.

on the time scale of tens of seconds corresponding to the effective T_1 given in Table I.

The effective T_2 is shown in Fig. 1 as a function of the fractional laser intensity fluctuation. At a FORT depth of $|U_m|=1$ mK and a relative intensity fluctuation of 10^{-4}, which is feasible with active stabilization and well above the limit set by quantum noise for mW power FORT beams, $T_2 \sim 12$ s.

Atomic motion within the FORT volume leads to a time varying trapping potential, and hence dephasing of the qubit states. This problem also arises in the context of precision measurements of optically trapped atoms [39,40]. A rough estimate says that since the atomic position spread is approximately $(T_a/|U_m|)^{1/2} w_{f0}/2$, the fractional variation in trapping intensity due to the transverse motion is $\sim T_a/2|U_m| \sim 0.025$ for the parameters of Table I. The same fractional variation is also found for the axial motion. This implies a motional variation in the hyperfine splitting of order 38 Hz. The maximum phase perturbation in one axial vibrational period is thus $\sim 2\pi \times 38$ Hz/3 kHz ~ 0.08 rad. We can also express this shift as an effective transverse relaxation time $T_2 \sim 1/38$ Hz $=0.026$ s.

This time is far shorter than the T_1 and T_2 times due to the other mechanisms discussed above. As has been demonstrated experimentally in Ref. [41], it is possible to cancel the differential ac Stark shift of the hyperfine states by introduction of a weak beam tuned between the hyperfine states that has the same spatial profile as the FORT beam. The intensity of the additional compensation beam can be very low such that the decoherence rates due to photon scattering will not change significantly. Kaplan *et al.* [41] demonstrated a reduction in transverse broadening by a factor of 50, and we assume that a factor of at least 100 is realistic, in order to arrive at the estimate of 2.6 s given in Table I. Additional discussion of motional effects in the context of single qubit operations is given in Sec. III.

F. Background magnetic and electric fields

The amount of dephasing caused by trapping and background field fluctuations depends on the qubit basis states that are used [13,39]. As shown in Fig. 2, for atoms with nuclear spin $I=3/2$ there are three possible choices of basis states that are first-order free of Zeeman shifts. In this subsection we consider the three possible choices and will conclude that set (a) is optimal for achieving long storage times with low decoherence.

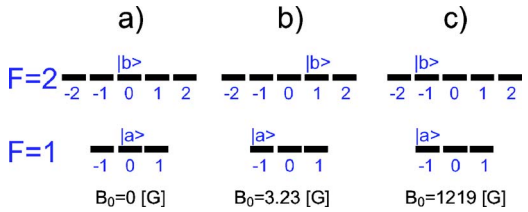

FIG. 2. (Color online) Possible choices of qubit basis states that have a magic bias field B_0 for which the relative Zeeman shift is a quadratic function of field fluctuations.

The simplest choice [Fig. 2(a)] is to use $|a\rangle=|F=1,m_F=0\rangle$ and $|b\rangle=|F=2,m_F=0\rangle$. Using the Breit-Rabi formula the second-order shift of the energy interval expressed as a frequency is

$$\omega_{ba} = \omega_{\rm hf}\left[1+\left(\frac{(g_S-g_I)\mu_B \delta B}{\hbar \omega_{\rm hf}}\right)^2\right]^{1/2}, \tag{19}$$

where $\omega_{\rm hf}$ is the zero-field hyperfine clock frequency between the $m_F=0$ states, μ_B is the Bohr magneton, g_S, g_I are the electron spin and nuclear Landé factors, and δB is the magnetic-field fluctuation. The frequency deviation $\delta\omega_{ba}=\omega_{ba}-\omega_{\rm hf}$ implies a transverse relaxation time $T_2=2\pi/\delta\omega_{ba}$ which evaluates to $T_2=1740$ s for $\delta B=1$ mG. While it is in principle possible to shield magnetic-field fluctuations to an even lower level it is difficult to do so in an experiment that requires substantial optical access to the atom trapping region. Recent work [42] has demonstrated suppression of static and fluctuating magnetic fields to the level of 300 μG using an active feedback scheme. We will assume 1 mG as a conservative estimate of the fluctuation level that can be achieved.

Alternatively we can use the states shown in Fig. 2(b): $|a\rangle=|F=1,m_F=-1\rangle$ and $|b\rangle=|F=2,m_F=1\rangle$. At a bias field of $B_0 \simeq 3.23$ G the frequency separation is quadratically dependent on fluctuations about B_0. A fluctuation of 1 mG about the bias point gives $T_2=2320$ s and frequency separations between the qubit basis states and neighboring Zeeman states of about 2.3 MHz.

Finally we could also use the states shown in Fig. 2(c): $|a\rangle=|F=1,m_F=-1\rangle$ and $|b\rangle=|F=2,m_F=-1\rangle$. At a bias field of $B_0=\hbar\omega_{\rm hf}/[2(g_S-g_I)\mu_B]$ the frequency separation is quadratically dependent on fluctuations about B_0. Defining $\delta B=B-B_0$ we have

$$\omega_{ba} = \frac{\sqrt{3}}{2}\omega_{\rm hf}\left[1+\frac{4}{3}\left(\frac{(g_S-g_I)\mu_B \delta B}{\hbar \omega_{\rm hf}}\right)^2\right]^{1/2}. \tag{20}$$

Apart from a factor of $2/\sqrt{3}$ larger sensitivity to fluctuations we retain the quadratic dependence of Eq. (19) at a very large bias field. For ^{87}Rb we find $B_0 \simeq 1219.3$ G and $T_2=1500$ s for $\delta B=1$ mG. At this large bias field the separation between neighboring m_F levels is hundreds of MHz. This large detuning will effectively suppress unwanted transitions during logic operations, but has the disadvantage of mixing

the hyperfine states so that there no longer will be a clean cycling transition between the $^2S_{1/2}|F=2,m_F=2\rangle$ and $^2P_{3/2}|F'=3,m_{F'}=3\rangle$ states that can be used for qubit measurement. One possibility would be to use a bias field that is applied during logic operations, and turned off adiabatically for state measurements.

The use of $m_F \neq 0$ basis states requires that we account for m_F dependent shifts due to the ground-state vector polarizability that couples to nonzero ellipticity of the trapping laser [39,43,44]. The energy shift can be written as

$$U_{\mathrm{ac}}^{(1)} = -\frac{1}{4}|\mathcal{E}_f|^2 \alpha_1 g_F m_F \sqrt{1-\epsilon^2}, \tag{21}$$

where $g_F=[F(F+1)+S(S+1)-I(I+1)]/[F(F+1)]$, m_F is the total spin projection along the FORT beam propagation direction $\hat{y}$, and the laser polarization is $\boldsymbol{\epsilon}=(1/\sqrt{2})(\hat{x}\sqrt{1+\epsilon}+i\hat{y}\sqrt{1-\epsilon})$. Basis states with $m_F=0$ have no vector shift, and in addition the field insensitive states $|0\rangle=|F=1,m_F=-1\rangle$ and $|1\rangle=|F=2,m_F=1\rangle$ both have $g_F m_F=1/2$ so there is no differential shift and no decoherence due to the vector polarizability. On the other hand, the choice $|0\rangle=|F=1,m_F=-1\rangle$ and $|1\rangle=|F=2,m_F=-1\rangle$ leads to a transverse decoherence time of $T_2=(\alpha_0/\alpha_1)(I/\delta I)2\pi\hbar/(k_B T_m\sqrt{1-\epsilon^2})$. Using the parameters given in the caption of Table I, $\epsilon=0.999$, and a fractional intensity fluctuation of $\delta I/I=0.001$, we find a short coherence time of $T_2=38$ ms. We see that it is important to avoid decoherence due to the vector polarizability so that the preferred choice is the qubit states shown in Figs. 2(a) and 2(b).

Careful analysis along the lines of that used in Sec. III shows that the set of Fig. 2(b) presents significant obstacles to achieving high fidelity single-qubit operations using stimulated two-photon Raman transitions. The essential problem is that the choice of Fig. 2(b) involves ground states separated by $|\Delta m_F|=2$. For large detunings the two-photon Raman rate for these transitions is proportional to the vector polarizability which has a selection rule $|\Delta m_F| \leqslant 1$. The Raman rate therefore vanishes so it is necessary to use two Raman beams with opposite helicities. In this situation the effective Raman rate scales as Δ_e/Δ_1^2 where Δ_e is the excited-state hyperfine splitting, and Δ_1 is the one-photon detuning of the Raman beams. However, the Raman beam induced ac Stark shifts scale as $1/\Delta_1$ so that in the limit of large detuning the ground-state ac Stark shifts become large compared to the Raman rate between ground states. It is not possible, without resorting to more complex polarization states, to balance the ac Stark shifts of the qubit basis states, which leads to entanglement of the qubit spin state with the atomic center-of-mass motion. This entanglement represents an undesired decoherence mechanism.

We are thus led to the choice shown in Fig. 2(a) for the qubit basis states. While the $m_F=0$ states are insensitive to magnetic fluctuations they are not optimal as qubit basis states at low magnetic fields. Atomic motion in a region of near zero magnetic field is subject to Majorana transitions between Zeeman sublevels. Transitions can be suppressed by Zeeman shifting the states with a bias magnetic field. Unfortunately a large bias field converts the small field quadratic dependence of Eq. (19) to a linear dependence on the field fluctuations about the bias point. For example, a bias field of 1 G, which gives MHz scale Zeeman shifts, with a fluctuation of 1 mG about the bias point would give $T_2=0.87$ s. We can do considerably better with a small 15-mG bias field, which is sufficient to suppress Majorana transitions, yet small enough such that with 1 mG of field fluctuations the coherence time is $T_2=56$ s. In the remainder of this paper we will analyze the implementation of quantum logic using the $m_F=0$ basis states.

Finally we note that dephasing due to dc electric fields is completely negligible. The T_2 due to differential ac Stark shifts calculated from Eq. (18) results from a peak electric field at the center of a mK deep optical FORT of $O[10^6(\mathrm{V/m})]$. Since we expect low-frequency field fluctuations to be much less than 1 V/m, the dc Stark shift can be neglected.

III. SINGLE-QUBIT OPERATIONS

A two-site FORT with a single atom loaded in each site provides a setting for studying basic one- and two-qubit operations. In this section we start with a study of the fidelity and decoherence properties of one-qubit operations at each site. Of particular concern will be the requirement of high fidelity operations at a targeted site without unintended disturbance of the neighboring site. Simply increasing the separation of the sites to reduce crosstalk will imply slow two-qubit conditional operations, so there is inevitably a performance tradeoff between one- and two-qubit gates. We discuss balancing the conflicting requirements in Sec. V below.

Single-qubit rotations between ground-state levels can be performed in several ways. Microwave fields that are resonant with ω_{ba} can be used, but do not allow direct single site addressing. By combining a microwave field with an electric- or magnetic-field gradient a selected site can be tuned into resonance [45]. The drawback of such an approach is that neighboring sites will be subjected to off-resonant perturbations.

Here we analyze an alternative approach using stimulated two-photon Raman transitions induced by tightly focused addressing beams, as shown in Fig. 3. Two-photon Raman techniques for laser cooling of neutral atoms were pioneered by Kasevich and Chu [46], and have been used recently in optical lattices by the group of Jessen [47] and others [48]. Raman techniques are also an important ingredient in trapped ion experiments [13]. As the physics of coherent-state manipulation with stimulated Raman pulses is well understood our aim here is to analyze a number of contributions to nonideal behavior that arise in the context of optically trapped atom experiments. The physical mechanisms contributing to nonideal single-qubit operations are summarized in Table II and discussed in Secs. III A–III E. In addition to qubit rotations fast state measurements are a requirement for error correction in a quantum processor. In Sec. III F we examine the speed and fidelity of single site state measurement using resonance fluorescence.

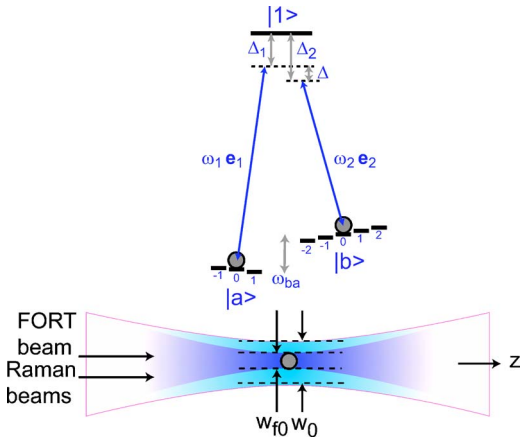

FIG. 3. (Color online) Single-qubit stimulated Raman rotations.

A. Speed and decoherence

As discussed in Sec. II the qubit logical basis states $|a\rangle, |b\rangle$ will be represented with the ^{87}Rb $5S_{1/2}|F=1, m_F=0\rangle$ and $|F=2, m_F=0\rangle$ ground-state hyperfine levels. Qubit initialization to the $|b\rangle$ state can be accomplished by driving the $5S_{1/2}(F=2)-5P_{3/2}(F'=2)$ transition with a beam linearly polarized along the magnetic field. An additional repumper beam returns atoms infrequently lost to the $F=1$ lower hyperfine manifold. When the transition is driven with an intensity several times larger than the saturation intensity population will accumulate in $|F=2, m_F=0\rangle$ at the rate of $\gamma/2$, where $\gamma/2\pi=5.98$ MHz is the spontaneous decay rate from the upper level. The characteristic qubit initialization time will be several transfer time constants, or ~ 0.1 μs. Experiments with atomic beams [49] have demonstrated preparation purity by optical pumping at the level of 10^{-4}.

Ground-state single qubit manipulations using stimulated Raman transitions can be performed with high fidelity and made quite free of decoherence due to spontaneous emission. The driving fields and atomic level structure are shown in Fig. 3. We consider two driving fields at frequencies ω_1, ω_2 with detunings $\Delta_1=\omega_1-\omega_{1a}$, $\Delta_2=\omega_2-\omega_{1b}$, and associated Rabi frequencies $\Omega_{1,2}=d_{1,2}\mathcal{E}_{1,2}/\hbar$, with $d_{1,2}$ the relevant dipole matrix elements between the ground states and the excited state $|1\rangle$. The fields propagate along the $\hat{z}$ axis with polarizations $\boldsymbol{\epsilon}_{1,2}$ so that the total optical field is

$$\mathbf{E} = \frac{e^{-r^2/w^2(z)}}{\sqrt{1+z^2/z_R^2}}\left[\frac{\mathcal{E}_1(t)}{2}e^{\imath(k_1 z-\omega_1 t)}\boldsymbol{\epsilon}_1 + \frac{\mathcal{E}_2(t)}{2}e^{\imath(k_2 z-\omega_2 t)}\boldsymbol{\epsilon}_2\right] + \text{c.c.}, \tag{22}$$

where $w(z)=w_0\sqrt{1+z^2/z_R^2}$, $z_R=\pi w_0^2/\lambda_R$, $\lambda_R=\lambda_1$, and we have taken the Rayleigh lengths of the two fields to be equal since $|(\lambda_1-\lambda_2)/(\lambda_1+\lambda_2)| \ll 1$.

Let us assume that the atom is in state $|a\rangle$ at $t=0$. The Raman light is tuned in the vicinity of either the $5P_{3/2}$ or $5P_{1/2}$ excited states. For definiteness we consider tuning near to the $5P_{1/2}$ excited state. In the limit of large single-photon detuning relative to the excited-state hyperfine structure the probability for the atom to be in state $|b\rangle$ at time t is

$$|c_b(t)|^2 = \frac{|\Omega_R|^2}{|\Omega_R|^2+\Delta^2}\sin^2\left(\frac{\sqrt{|\Omega_R|^2+\Delta^2}}{2}t\right), \tag{23}$$

where $\Omega_R=\Omega_1\Omega_2^*/\delta$, $\delta=\Delta_1+\Delta_2$, and $\Delta=\omega_1-\omega_2-\omega_{ba}+(|\Omega_2|^2-|\Omega_1|^2)/(2\delta)$. When $|\Delta| \ll |\Omega_R| \ll |\Delta_1|, |\Delta_2|$ we have $\delta \simeq 2\Delta_1$ and the effective Rabi frequency is $\Omega_R \simeq \Omega_1\Omega_2^*/(2\Delta_1)$. We assume that Δ_1, Δ_2 are small compared to the ^{87}Rb fine structure splitting of 7120 GHz, so we neglect any contribution from the other $5P$ state.

The probability of spontaneous emission during a π pulse of time $t_\pi=\pi/\Omega'$, with $\Omega'=\sqrt{|\Omega_R|^2+\Delta^2}$ the effective off-resonance Rabi frequency, is $p_{se}=\tau^{-1}\int_0^{t_\pi} dt|c_p(t)|^2$, where c_p is the amplitude of the excited state and $\tau=27.7$ ns is the $5P_{1/2}$ lifetime. Neglecting the two-photon detuning and assuming a piecewise constant pulse profile it is readily shown that p_{se}

TABLE II. Physical mechanisms contributing to imperfection of single-qubit operations. The decoherence probability is calculated for a π rotation, and the fidelity error is calculated with respect to an ideal $\pi/2$ rotation using the metric of Eq. (26). Values listed are for $T_m=1$ mK, $T_a=50$ μK, $\lambda_f=1.01$ μm, $w_{f0}=2.5$ μm, and $w_0=5$ μm. See text for details.

Mechanism	Section	p_{dch}	Error
Spontaneous emission	III A	9×10^{-5}	
ac stark shifts	III B		4.4×10^{-7}
Atomic motion	III C		9.4×10^{-5}
Spatial crosstalk	III C		2.2×10^{-5}
Polarization leakage	III D	9.7×10^{-5}	
Laser intensity noise	III E		9.4×10^{-8}
Laser phase noise	III E		2.5×10^{-7}
Combined		1.9×10^{-4}	1.2×10^{-4}

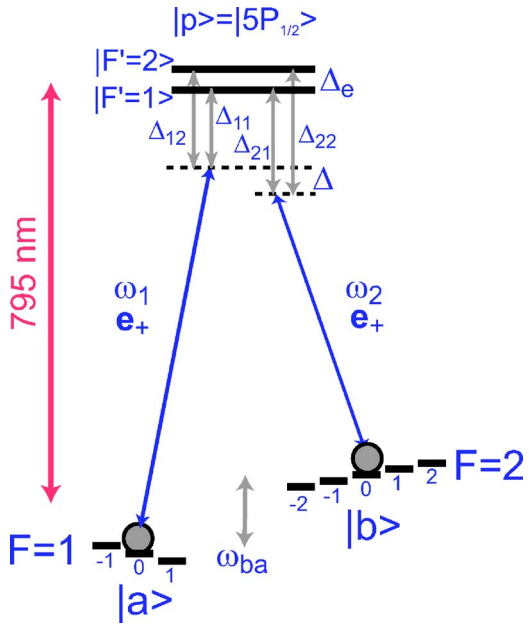

FIG. 4. (Color online) Stimulated Raman rotations with two excited states.

$\simeq \pi/(2|\Delta_1|\tau)$. For ^{87}Rb with $\Delta_1/2\pi=-100$ GHz we get $p_{se}=9\times10^{-5}$.

The speed of two-photon Raman transitions scales with the optical intensity. In subsequent sections we will be concerned with corrections to the effective Raman frequency due to the excited-state hyperfine structure shown in Fig. 4. We work in the limit of $|\Delta| \ll |\Omega_R| \ll |\Delta_{11}|, |\Delta_{12}|, |\Delta_{21}|, |\Delta_{22}|$, so the excited states are weakly populated. With $\mathbf{e}_1=\mathbf{e}_2=\mathbf{e}_+$ the effective Rabi frequency is

$$|\Omega_R| = \frac{2e^2(R_{5S,5P})^2}{\epsilon_0 c\hbar^2} KI \left| \frac{\Delta_{11}-\Delta_e/4}{2\Delta_{11}(\Delta_{11}-\Delta_e)} \right|, \tag{24}$$

with $R_{5S,5P}\simeq 5.13a_0$ the radial integral between the ground and excited states, a_0 is the Bohr radius, $K=1/9$ is an angular factor, I is the intensity of each Raman beam, and $\Delta_e/2\pi=817$ MHz is the hyperfine splitting of the excited state. Working with 100 μW in each beam focused to a spot with waist $w_0=5$ μm at a detuning of $|\Delta_{11}|/2\pi=100$ GHz we get $\Omega_R/2\pi=4.6$ MHz.

B. Raman beam ac Stark shifts

In this section we calculate heating and decoherence effects due to the tightly focused Raman beams. Before proceeding with calculations of the fidelity of qubit operations we define the metric to be used. Starting with an initial pure state $|\psi\rangle=c_a|a\rangle+c_b|b\rangle$ a two-photon stimulated Raman transition results in the transformation $|\psi\rangle\rightarrow R(\Omega_R,\Delta,t)|\psi\rangle$ where the rotation matrix is

$$R(\Omega_R,\Delta,t) = \begin{pmatrix} e^{\imath\Delta t/2}\left[\cos\left(\frac{\Omega' t}{2}\right) - i\frac{\Delta}{\Omega'}\sin\left(\frac{\Omega' t}{2}\right)\right] & ie^{\imath\Delta t/2}\frac{\Omega_R^*}{\Omega'}\sin\left(\frac{\Omega' t}{2}\right) \\ ie^{-\imath\Delta t/2}\frac{\Omega_R}{\Omega'}\sin\left(\frac{\Omega' t}{2}\right) & e^{-\imath\Delta t/2}\left[\cos\left(\frac{\Omega' t}{2}\right) + i\frac{\Delta}{\Omega'}\sin\left(\frac{\Omega' t}{2}\right)\right] \end{pmatrix}. \tag{25}$$

In writing Eq. (25) we have suppressed a multiplicative phase factor and neglected a small correction to some of the terms containing Δ that is proportional to the differential ac Stark shift of the basis states. The fidelity of a rotation operation $R(\Omega_R,\Delta,t)$ compared to an ideal transformation with $R_0=R(\Omega_{R0},\Delta_0,t_0)$ can be defined as

$$F = \langle |\langle R_0\psi|R\psi\rangle|^2\rangle, \tag{26}$$

where the outer brackets specify an average over any stochastic contributions to R.

In the simplest case of two-photon resonance $\Delta=0$ and the rotation matrix simplifies to

$$R(\theta,\phi) = \begin{pmatrix} \cos(\theta/2) & ie^{-\imath\phi}\sin(\theta/2) \\ ie^{\imath\phi}\sin(\theta/2) & \cos(\theta/2) \end{pmatrix}, \tag{27}$$

where $\theta=|\Omega_R|t$ and $\phi=\arg(\Omega_R)$. For the particular case of an ideal π pulse ($\theta_0=\pi$, $\phi_0=0$) with $|\psi\rangle=|a\rangle$ the fidelity is $F=(1/2)(1-\cos\theta)$. As this metric is independent of errors in the azimuthal angle ϕ we find it more informative to quantify the fidelity of a single operation with respect to an ideal $\pi/2$ pulse. In this case the fidelity is $F=(1/2)(1+\cos\phi\sin\theta)$. The gate errors listed in Table II are defined by $E=1-F$. The extent to which errors accumulate in concatenated qubit operations is an important consideration when designing a computational sequence. A discussion of this topic in the context of an ion trap experiment has been given in Ref. [13].

Returning to the effect of ac Stark shifts we note that in addition to providing controlled rotations between the qubit basis states the Raman beams result in unequal ac Stark shifts of the Zeeman states which leads to an additional rotation phase $\delta\phi$. The rotation phase has an average value that must be accounted for [50], as well as a stochastic part resulting from atomic motion that leads to a fidelity error. The Raman beam induced Stark shifts also play a useful role by enhancing the nondegeneracy of the Zeeman states beyond that provided by the very small bias magnetic field. This effect greatly reduces leakage out of the computational basis as we discuss in Sec. III D below.

In order to give a quantitative account of the ground-state Stark shifts for Raman beams tuned near the D1 line we add the contributions from the $|F'=1,2\rangle$ excited states for both beams to get the results shown in Table III. Using the physical parameters given in the previous section we find the change in trapping potential at the center of one of the Raman beams is $U_R\sim 220$ μK which is a few times less than the $|U_m|=1$ mK wells created by the FORT beams. Using red detuned Raman beams the additional potential is attractive, nonetheless, the associated dipole forces can lead to heating of the trapped atoms. In the limit where the Rabi frequency is much larger than the trap oscillation frequency a trapped atom will only move a small fraction of its orbit during a Raman pulse. The dipole force during the pulse will with equal probability accelerate or decelerate the atomic motion, so that on average, to lowest order in the ratio of trap frequency to Rabi frequency, there will be no heating. Another way to see this is to note that the heating rate given by Eq. (13) vanishes when the perturbation has no energy at twice the trap oscillation frequency.

Nonetheless, when we consider the effect of a single Rabi pulse there will be a worst case heating of the atomic motion that we require to be small compared to the trap depth to avoid loss of the trapped atom. It is readily shown that the heating due to a single Rabi π pulse is bounded by δU

TABLE III. Stark shifts of Zeeman ground states due to the Raman beams of Fig. 4. The Stark shifts given by $\delta U_R=[e^2R^2_{5S,5P_{1/2}}/(\epsilon_0 c\hbar)](K/72)I$, with I the intensity of each Raman beam, are evaluated in columns 3 and 4 for $I=100\ \mu$W and $\Delta_{11}/2\pi=-100$ GHz.

Ground state	K	δU_R(mK)	$[\delta U_R-\delta U_R(\lvert a\rangle)]/h$(MHz)
$\lvert 1-1\rangle$	$\frac{1}{\Delta_{11}}+\frac{1}{\Delta_{11}-\Delta_e}+\frac{1}{\Delta_{11}-\omega_{ba}}+\frac{1}{\Delta_{11}-\Delta_e-\omega_{ba}}$	−0.107	−2.41
$\lvert 10\rangle(=\lvert a\rangle)$	$\frac{1}{\Delta_{11}}+\frac{3}{\Delta_{11}-\Delta_e}+\frac{1}{\Delta_{11}-\omega_{ba}}+\frac{3}{\Delta_{11}-\Delta_e-\omega_{ba}}$	−0.213	0
$\lvert 11\rangle$	$\frac{6}{\Delta_{11}-\Delta_e}+\frac{6}{\Delta_{11}-\Delta_e-\omega_{ba}}$	−0.319	2.42
			$[\delta U_R-\delta U_R(\lvert b\rangle)]/h$(MHz)
$\lvert 2-2\rangle$	$\frac{6}{\Delta_{11}+\omega_{ba}}+\frac{2}{\Delta_{11}-\Delta_e+\omega_{ba}}+\frac{6}{\Delta_{11}}+\frac{2}{\Delta_{11}-\Delta_e}$	−0.458	−4.79
$\lvert 2-1\rangle$	$\frac{3}{\Delta_{11}+\omega_{ba}}+\frac{3}{\Delta_{11}-\Delta_e+\omega_{ba}}+\frac{3}{\Delta_{11}}+\frac{3}{\Delta_{11}-\Delta_e}$	−0.343	−2.39
$\lvert 20\rangle(=\lvert b\rangle)$	$\frac{1}{\Delta_{11}+\omega_{ba}}+\frac{3}{\Delta_{11}-\Delta_e+\omega_{ba}}+\frac{1}{\Delta_{11}}+\frac{3}{\Delta_{11}-\Delta_e}$	−0.228	0
$\lvert 21\rangle$	$\frac{2}{\Delta_{11}-\Delta_e+\omega_{ba}}+\frac{2}{\Delta_{11}-\Delta_e}$	−0.114	2.38
$\lvert 22\rangle$	0	0	4.75

$=2\pi U_R(w_{f0}^2/2w_0^2)(T_a/|U_m|)(\omega_x/\Omega_R)$. Using the parameters given in Tables I and II and $\Omega_R=2\pi\times 4.6$ MHz, we find $\delta U\sim 70$ nK. Since this amount of heating is very small compared to the FORT depth, it will not lead to escape of the trapped atom. Note that in the limit of fast Rabi frequency the amount of heating is proportional to the atomic temperature, but is independent of the laser intensity used for the Raman pulse. Although in the first approximation the heating per Rabi rotation averages to zero there is a contribution to the heating rate proportional to the square of the trap frequency. For $T_a=50\ \mu$K we get an average energy increase of 70 nK per operation so the maximum number of operations before there is significant heating of the atoms is about 10^3. This implies that recooling of the atomic motion after state measurements will be necessary to enable many logical operations. In principle recooling, and reinitialization of a qubit to a fiducial state can be done on a site specific basis using tightly focused molasses beams for Doppler cooling, or Raman sideband cooling in a tightly confining optical trap.

To quantify the fidelity error due to the Raman beam induced ac Stark shifts we note that a Rabi rotation will result in a transformation $|\psi\rangle=c_a|a\rangle+c_b|b\rangle\rightarrow c'_a|a\rangle+e^{i\delta\phi}c'_b|b\rangle$, where c'_a, c'_b are the desired result of the Rabi rotation, and $\delta\phi$ is an additional differential phase shift due to the ac Stark shifts. The differential phase can be written as $\delta\phi=\delta\phi_b-\delta\phi_a=t(\delta U_b-\delta U_a)/\hbar$ with t the length of the pulse. The Raman field $\mathcal{E}$ that is seen by the trapped atom is time dependent due to the atomic motion at finite temperature. The time averaged differential phase is proportional to $\langle\delta\phi\rangle\sim\langle\mathcal{E}^2\rangle$ and the variance of the phase shift is $\Delta^2(\delta\phi)=\langle\delta\phi^2\rangle-\langle\delta\phi\rangle^2$. Accounting for the atomic motion in the two transverse dimensions, and neglecting the axial motion which gives a much smaller contribution to time variation of the field, we find $\langle\mathcal{E}^2\rangle=\mathcal{E}_0^2/[1+(T_a/|U_m|)(w_{f0}/w_0)^2]$ and $\langle\mathcal{E}^4\rangle=\mathcal{E}_0^4/[1+2(T_a/|U_m|)(w_{f0}/w_0)^2]$, with $\mathcal{E}_0$ the peak value of the field. These expressions are valid in the limit of tight confinement where $T_a\ll|U_m|$.

Using Eq. (24) and Table III we find to leading order in the ratio of the atomic temperature to the trap depth for a $\pi/2$ pulse of length $t_{\pi/2}=\pi/2\langle|\Omega_R|\rangle$,

$$\langle\delta\phi\rangle=-\frac{\pi}{2}\frac{\omega_{ba}}{\Delta_{11}}-\frac{3\pi}{8}\frac{\Delta_e\omega_{ba}}{\Delta_{11}^2}+O(\omega_{ba}^3/\Delta_{11}^3), \tag{28a}$$

$$\Delta^2(\delta\phi)=\left(\frac{T_a}{|U_m|}\right)^2\left(\frac{w_{f0}}{w_0}\right)^4\left|\frac{\pi}{2}\frac{\omega_{ba}}{\Delta_{11}}+\frac{3\pi}{8}\frac{\Delta_e\omega_{ba}}{\Delta_{11}^2}+O(\omega_{ba}^3/\Delta_{11}^3)\right|^2. \tag{28b}$$

The average phase shift given by Eq. (28a) evaluates to 0.1 rad for $\Delta_{11}/2\pi=-100$ GHz. This phase can be compensated for by adjustment of the relative phase of the Raman beams. It turns out using the full dependence of differential phase on detuning that there are finite values of the detuning such that the ac Stark shifts are equal and the differential phase vanishes [51]. However, these detunings are of order the hyperfine ground-state splitting, and are too small to suppress

spontaneous emission from the $5P_{1/2}$ states. The standard deviation of the stochastic phase given by Eq. (28b) scales linearly with the factor $(T_a/|U_m|)(w_{f0}/w_0)^2$ which expresses the amount of variation of the Raman intensity over the cross sectional area to which the atom is confined. Using Eq. (26) the gate error is $E \simeq (1/4)\Delta^2(\delta\phi) = 4.4\times10^{-7}$ at -100-GHz detuning.

C. Atomic position and velocity fluctuations

In addition to fluctuations in the phase of the Rabi rotation, variations in the atomic position and velocity also directly perturb the angle of single-qubit rotations since the effective pulse area depends on the local value of the Raman beam intensities as well as motional detuning due to Doppler shifts. Starting with an atom in state $|a\rangle$, and applying the Raman fields $\mathcal{E}_1, \mathcal{E}_2$ the probability for the atom to be rotated to state $|b\rangle$ after time t is given by Eq. (23). Fluctuations in the atomic position and momentum lead to fluctuations in the effective pulse area at time t_π.

We can characterize a $\pi/2$ pulse and its fluctuations due to atomic motion by

$$\langle|\Omega_R|t_{\pi/2}\rangle = \pi/2, \quad \langle|\Omega_R|^2 t_{\pi/2}^2\rangle = \pi^2/4 + \langle\epsilon_1^2\rangle, \tag{29}$$

$$\langle\Delta t_{\pi/2}\rangle = 0, \quad \langle\Delta^2 t_{\pi/2}^2\rangle = \langle\epsilon_2^2\rangle, \tag{30}$$

where we have assumed the system has been prepared with zero detuning and ϵ_1, ϵ_2 are small stochastic parameters. With the Raman beams copropagating the two-photon detuning is first order Doppler free. Taking account of the velocity spread given by Eq. (6c) we find

$$\langle\epsilon_2^2\rangle = \frac{\pi^2\omega_{ba}^2}{4c^2\Omega_R^2}\frac{T_a}{m}. \tag{31}$$

At $T_a = 50$ μK we find $\langle\epsilon_2^2\rangle \simeq 3\times10^{-13}$ so we can neglect the contribution of Doppler detuning to the rotation error and use the simplified rotation matrix of Eq. (27) with $\phi = 0$.

Averaging over the atomic motion in the same way as in the previous section we find

$$\langle\epsilon_1^2\rangle = \frac{\pi^2}{4}\left(\frac{T_a}{T_m}\right)^2\left(\frac{w_{f0}}{w_0}\right)^4 \tag{32}$$

and a fidelity error of $E = (1/4)\langle\epsilon_1^2\rangle$. This result takes account of the two-dimensional transverse motion of the trapped atom. Adding in the axial motion gives an additional factor proportional to ξ_f^2/ξ^2, where $\xi = \pi w_0/\lambda_R$. Our standard system parameters give $\xi_f^2/\xi^2 = 0.15$, so this is a small correction which we will neglect. With the parameters of Table II we find $E = 9.4\times10^{-5}$ at a temperature of $T_a = 50$ μK. This error is larger than that due to ac Stark shifts by a factor of $(\Delta_{11}/\omega_{ba})^2$, but is still very small at typical sub-Doppler temperatures that are easily reached in a MOT.

As the motional error scales inversely with the waist of the Raman beams it is desirable to use as large a waist as possible. In a multiple site device unwanted crosstalk occurs if the waist is made comparable to the site to site spacing d. Simply increasing d is not feasible since that would reduce the fidelity of two-qubit operations, as will be discussed in Sec. IV. The application of Raman beams giving a Rabi frequency Ω_R at the addressed qubit will result in a leakage Rabi frequency at a neighboring qubit of $\Omega_R' = \Omega_R e^{-2d^2/w_0^2}$. For parameters that give a $\pi/2$ rotation at the targeted site there will be a fidelity error of $E = (\pi^2/16)e^{-4d^2/w_0^2}$ at the neigboring site. We will use a site spacing of $d = 8$ μm which gives $E = 2.2\times10^{-5}$ for $w_0 = 5$ μm. In practice laser beams that pass through a large number of optical elements may deviate significantly from an ideal Gaussian profile. Full characterization of spatial crosstalk will depend on specific experimental details.

D. Polarization effects

Two-photon stimulated Raman transitions may result in the atom being transferred to a Zeeman state that lies outside the computational qubit basis. This will occur when the Raman beams are a mixture of polarization states. The connection between fidelity loss due to unwanted transitions and the polarization impurity δ of the Raman beams is calculated in the Appendix. With careful attention to optical design we may achieve $\delta \sim 10^{-3}$ for a wide beam. In order to control one qubit at a time the Raman beams are focused to a waist of $w_0 = 5$ μm. Near the focus of a linearly polarized Gaussian beam propagating along $\hat{z}$ the positive frequency component of the field can be written as $\mathbf{E}(x,y,z,t) = \mathbf{e}_x(\mathcal{E}_0/2)e^{-(x^2+y^2)/w_0^2}e^{i(kz-\omega t)}$. Consistency with Maxwell's equations requires that the actual field is $\mathbf{E}(x,y,z,t) = [\mathbf{e}_x - i(x/z_R)\mathbf{e}_z](\mathcal{E}_0/2)e^{-(x^2+y^2)/w_0^2}e^{i(kz-\omega t)}$ which includes a component of $\mathbf{e}_z$. Thus a circularly polarized field, $\mathbf{E} \sim \mathbf{e}_+$ becomes $\mathbf{E}(x,y,z,t) = [\mathbf{e}_+ + [(y-ix)/z_R]\mathbf{e}_0](\mathcal{E}_0/2)e^{-(x^2+y^2)/w_0^2}e^{i(kz-\omega t)}$. We can make a rough estimate of the magnitude of the polarization induced leakage by inserting into Eqs. (A1) and (A2) $|\epsilon_{ij}| \simeq \sqrt{\langle x_a^2\rangle}/z_R = [w_{f0}/(kw_0^2)]\sqrt{T_a/|U_m|} = 0.0028$, with the numerical value calculated for our standard parameters and $T_a = 50$ μK. This estimate puts an upper limit on the effective polarization purity in the interaction region, even when the unfocused Raman beams are perfectly polarized. Using this value for all coefficients ϵ gives the last column in Table VI which shows that transition amplitudes to undesired states will not exceed $\sim 6.6\times10^{-3}$. Leakage out of the computational basis is a source of decoherence. We characterize the decoherence probability for a π pulse by adding the probabilities for leakage out of states $|a\rangle$ or $|b\rangle$. We find starting in $|a\rangle$ a leakage probability of 5.6×10^{-5}, and starting in $|b\rangle$ 9.4×10^{-5}. We use the larger of these numbers in Table II as an estimate of the decoherence probability due to polarization effects.

E. Laser intensity noise and linewidth

Intensity fluctuations of the Raman lasers will impact the accuracy of the Rabi pulse area. With the average intensity and pulse length set to give a $\pi/2$ pulse, a relative fluctuation of $\delta I/I$ implies a fidelity error of $E = (1/4)(\delta I/I)^2$. Active stabilization of the Raman laser intensity is limited by shot noise to [13]

$$\frac{\delta I}{I} \geqslant \left(\frac{4\hbar\omega_1}{\eta P t_{\pi/2}}\right)^{1/2},$$

where P is the power of the Raman beam and η is the quantum efficiency of the detector in the stabilization circuit. With $P=100\ \mu$W, $|\Omega_R|/2\pi=4.6\times10^6$ Hz, and $\eta=0.5$ we find $\delta I/I\geqslant10^{-4}$ and $E\geqslant9.4\times10^{-8}$.

Finite laser linewidth, and in particular relative phase fluctuations of the two Raman beams will lead to errors in the phase ϕ of the qubit rotation. Laser oscillators have been demonstrated with a fractional frequency instability of 3×10^{-16} at 1 sec averaging time [52]. An optical phase lock between two laser oscillators with a residual phase noise at the 1 μrad level has also been achieved [53]. As a conservative estimate we will assume the Raman lasers can be prepared with a relative phase noise of 1 mrad. This implies a fidelity error for a $\pi/2$ rotation of $E=2.5\times10^{-7}$.

F. State detection using resonance fluorescence

Rapid state selective measurements can be made by illuminating the atom with $\mathbf{e}_+$ polarized light tuned close to the $|5S,F=2,m_F=2\rangle\leftrightarrow|5P,F=3,m_F=3\rangle$ cycling transition. State readout can be based on detection of resonance fluorescence [54]. Alternatively amplitude [55] and/or phase shifts imparted to a tightly focused probe beam can be used. In either case Poissonian photon counting statistics result in measurement times that are several orders of magnitude longer than Rydberg gate operation times. While the use of sub-Poissonian light could be advantageous in this context, it would add additional complexity.

It is of interest to estimate the time for performing a state measurement with a desired accuracy. The number of photon counts recorded in a measurement time τ is

$$q(\tau)=\eta\frac{\Omega_d}{4\pi}\frac{\gamma\tau}{2}\frac{I/I_s}{1+4\frac{\Delta^2}{\gamma^2}+I/I_s}, \tag{33}$$

where Ω_d is the solid angle of the collection optics, γ is the radiative linewidth, I is the readout intensity, I_s is the saturation intensity, and Δ is the detuning of the readout light from the cycling transition. The factor $\eta<1$ accounts for the quantum efficiency of the detector as well as any optical losses. The counts are assumed poisson distributed so that the probability of measuring n counts is $P_n(q)=e^{-q}q^n/n!$. We also assume a background count rate b_0 due mainly to parasitic scattering from optical components and detector dark counts that gives a count number $b(\tau)=b_0\tau$.

To make a measurement we detect scattered photons for a time τ. If the number of counts is greater than or equal to a cutoff number n_c we have measured the qubit to be in state $|b\rangle$. The measurement is incorrect if the actual number of signal counts was less than n_c or the number of background counts was greater than or equal to n_c. The probability of a measurement error is therefore

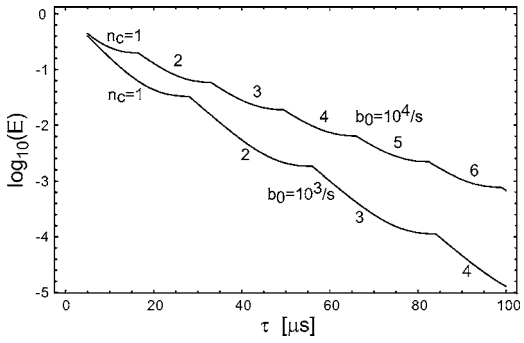

FIG. 5. State detection by resonance fluorescence for two different background count rates. The curves are labeled with the optimum values of n_c. Parameters used were $\Omega_d/4\pi=0.05$, $\Delta/\gamma=-1/2$, $I/I_s=1$, $\gamma=2\pi\times6$ MHz, and $\eta=0.6$.

$$E=\sum_{n=0}^{n_c-1}P_n(q)+\sum_{n=n_c}^{\infty}P_n(b)=1-\frac{\Gamma(n_c,b)}{\Gamma(n_c)}+\frac{\Gamma(n_c,q)}{\Gamma(n_c)}, \tag{34}$$

where $\Gamma(n_c)=(n_c-1)!$ and $\Gamma(n_c,q)=\int_q^\infty dt\ t^{n_c-1}e^{-t}$ is the incomplete gamma function. Since $\Gamma(n_c,0)=\Gamma(n_c)$ the error vanishes when $b\to0$ and $q\to\infty$. For given values of q and b there is an optimum choice of n_c that minimizes the error.

Figure 5 shows the error probability as a function of measurement time for experimentally realistic parameters. We see that optimum detection corresponds to a very small value for n_c and that even with background rates as high as $b_0=10^4\ \mathrm{s}^{-1}$ accurate measurements can be made in under 100 μs. A problematic aspect of the state measurement process is concomitant heating of the atomic motion. The calculations shown assume a detuning of $\Delta=-\gamma/2$, so that if counterpropagating readout beams are used it should be possible to cool the atomic motion while performing the measurement. Experiments have demonstrated the feasibility of long measurement times exceeding several seconds for single atoms confined in micron sized optical traps [32,56].

IV. TWO-QUBIT PHASE GATE

In this section we study the performance of the Rydberg gate using the geometry of two trapped atoms separated by a distance R, as shown in Fig. 6. The basic idea of the Rydberg gate is to use the strong dipole-dipole interaction of highly excited atoms to give a fast conditional phase shift. The fidelity of a conditional two-qubit operation will be impacted by the mechanisms affecting single-qubit gates listed in Table II, plus additional effects specific to the use of Rydberg states. As was shown above the single-qubit imperfections can be quite small, leading to projected fidelity errors $O(10^{-4})$. In the following subsections we analyze the additional errors specific to a conditional phase gate.

In comparison to the performance of single-qubit operations there are two significant complications involved in achieving conditional logic. The first is that optical excitation of Rydberg levels cannot readily be made Doppler free so that atomic motion introduces pulse area errors. The second,

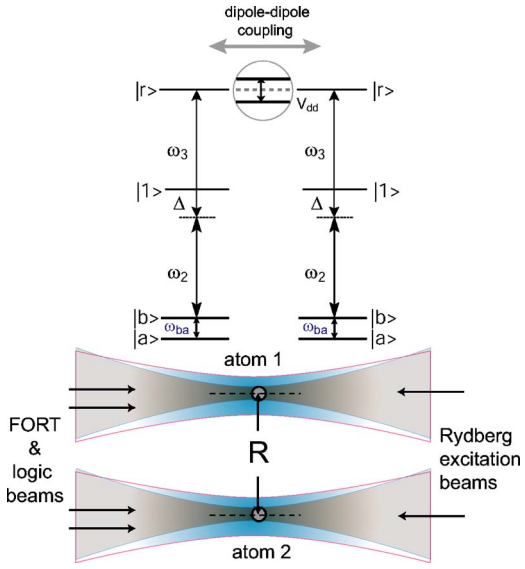

FIG. 6. (Color online) Geometry of two-qubit interactions.

and more serious limitation, arises from motional heating due to transfer to Rydberg states, and decoherence due to the finite lifetime of the Rydberg states. We present a solution to the heating problem based on balancing ground- and Rydberg-state polarizabilities, and show that the decoherence rates can be managed such that high fidelity gate operations appear possible.

The Rydberg gate can be optimized in two limits. In the first limit (Sec. IV A), where the atoms are relatively far apart, the two-atom interaction frequency shift is small compared to the Rabi frequency of the Rydberg-state excitation. In the opposite limit of closely spaced atoms (Sec. IV B) the dipole-dipole interaction is large compared to the Rabi frequency. In both cases the finite lifetime of the Rydberg state sets a lower limit on the gate fidelity that scales as the smaller of $(\Omega_R\tau)^{-2/3}$ or $(\Delta_{dd}\tau)^{-2/3}$, with Ω_R the Rabi frequency of the Rydberg excitation, Δ_{dd} the dipole-dipole interaction shift, and τ the excited-state lifetime.

We start the analysis of the phase gate by calculating its intrinsic fidelity scaling with speed of operation. The dipole-dipole interaction energy is

$$V_{dd} = \hbar\Delta_{dd} = \frac{1}{4\pi\epsilon_0 R^3}\left[\boldsymbol{\mu}_1\cdot\boldsymbol{\mu}_2 - 3\frac{(\boldsymbol{\mu}_1\cdot\mathbf{r}_{12})(\boldsymbol{\mu}_2\cdot\mathbf{r}_{12})}{R^2}\right]. \tag{35}$$

Here $\boldsymbol{\mu}_j$ is the dipole moment of atom j, and $\mathbf{r}_{12}=R\hat{\mathbf{r}}_{12}$ is the atomic separation. When the site to site qubit spacing R is sufficiently large the dipole-dipole interaction shift Δ_{dd} is a small perturbation compared to Ω_R, the Rabi frequency for excitation from $|b\rangle\rightarrow|r\rangle$. The protocol for a phase gate in this limit is [21] (i) excite both atoms from $|b\rangle\rightarrow|r\rangle$ with a π pulse, (ii) wait a time $t_{dd}=\pi/\Delta_{dd}(R)$, and (iii) transfer both atoms back down from $|r\rangle\rightarrow|b\rangle$ with a π pulse. Here $\Delta_{dd}(R)$ is the dipole-dipole shift at an atomic spacing of R. The resulting idealized logic table is $|aa\rangle\rightarrow|aa\rangle$, $|ab\rangle\rightarrow-|ab\rangle$, $|ba\rangle\rightarrow-|ba\rangle$, $|bb\rangle\rightarrow-|bb\rangle$ which is an entangling phase gate. Adding single-qubit Hadamard gates before and after the conditional interaction implements a controlled-NOT gate. The fidelity of the gate is constrained by the presence of four time scales. In the large Rabi frequency limit we have $1/\omega_{ba}\ll 1/|\Omega_R|\ll 1/\Delta_{dd}\ll\tau$, where input state decoherence error rotation error τ is the natural lifetime of the Rydberg state. The fidelity is fundamentally limited by the combination $\omega_{ba}\tau$ which should be as large as possible. Using characteristic values of $\omega_{ba}=2\pi\times 6835$ MHz and $\tau=100$ μs gives $\omega_{ba}\tau\sim 4\times 10^6$ which is sufficiently large for high fidelity operation.

There is an intrinsic source of error in this gate that scales with the ratio Δ_{dd}/Ω_R. Assume that the Raman fields used for the $|b\rangle\rightarrow|r\rangle$ transfer provide a π pulse when at most one of the atoms is excited to $|r\rangle$. Then if both atoms start in state $|b\rangle$ the excitation to $|r\rangle$ will be imperfect due to the dipole-dipole shift. In this case the gate operation will end with a small amplitude for the atoms to remain in state $|rr\rangle$. It is readily shown that the probability for this to happen, and hence the gate error, is $E\sim(\Delta_{dd}/\Omega_R)^2$. This error is intrinsic to the design of the gate, so we require a ratio of interaction shifts to Rabi frequency of 0.1, or less, for high fidelity operation.

Unfortunately, the finite lifetime of the Rydberg state gives a finite decoherence rate, and an error that grows linearly with the time of the gate. As the gate time scales with $1/\Delta_{dd}$ the interaction must be sufficiently strong to achieve high fidelity. We can write the probability of decoherence as $P\sim t_{dd}/\tau=\pi/\tau\Delta_{dd}$ where τ is the excited-state lifetime due to all decay mechanisms (see Secs. IV E and IV F). The total gate error accounting for both imperfect fidelity and decoherence is then $E\sim(\Delta_{dd}/\Omega_R)^2+1/(\tau\Delta_{dd})$. The error is minimized for $\Delta_{dd}\sim(\Omega_R^2/\tau)^{1/3}$, which then gives $E\sim(1/\tau\Omega_R)^{2/3}$. We see that the excited-state lifetime dictates how fast the Rydberg excitation must be performed to achieve a desired error level.

A. Large Rabi frequency

In this section we investigate operation in the large Rabi frequency limit in detail. To quantify the fidelity error we average over the four possible initial states of the phase gate which gives the results shown in Table IV. The calculations are performed using the rotation matrix of Eq. (25) and the fidelity definition of Eq. (26). The decoherence error listed in the table is the integrated probability of a transition out of the Rydberg state during the gate operation due to spontaneous emission or other mechanisms. For example the decoherence error for each atom with the initial condition $|aa\rangle$ is $E\simeq(2/\tau)\int_0^{\pi/|\Omega_R|}dt(|\Omega_R|^2/\Omega'^2)\sin^2(\Omega' t/2)+\pi/(\Delta_{dd}2\tau)$, with $\Omega'=\sqrt{|\Omega_R|^2+\omega_{ba}^2}$. The error is then doubled to account for two atoms.

The rotation error corresponds to the probability that the atom is in the Rydberg state at the end of the gate. For the initial condition $|bb\rangle$ the two-atom error is

$$E = 1 - \left|\begin{pmatrix}1\\0\end{pmatrix}^T R(\Omega_R,\Delta_{dd},\pi/|\Omega_R|)\begin{pmatrix}1 & 0\\ 0 & -1\end{pmatrix} \times R(\Omega_R,\Delta_{dd},\pi/|\Omega_R|)\begin{pmatrix}1\\0\end{pmatrix}\right|^4. \tag{36}$$

Here the rotation matrices operate on the states $|b\rangle$ and $|r\rangle$

TABLE IV. Leading contributions to the fidelity errors of a phase gate in the large Rabi frequency limit. See text for details.

Input state	Decoherence error	Rotation error
$\|aa\rangle$	$\frac{2\pi\|\Omega_R\|}{\tau\omega_{ba}^2}\left(1+\frac{\|\Omega_R\|}{2\Delta_{dd}}\right)$	$\frac{2\|\Omega_R\|^2}{\omega_{ba}^2}$
$\|ab\rangle$ or $\|ba\rangle$	$\frac{\pi\|\Omega_R\|}{\tau\omega_{ba}^2}\left(1+\frac{\|\Omega_R\|}{2\Delta_{dd}}\right)+\frac{\pi}{\tau\Delta_{dd}}\left(1+\frac{\Delta_{dd}}{\|\Omega_R\|}\right)$	$\frac{\|\Omega_R\|^2}{\omega_{ba}^2}$
$\|bb\rangle$	$\frac{2\pi}{\tau\Delta_{dd}}\left(1+\frac{\Delta_{dd}}{\|\Omega_R\|}\right)$	$\frac{8\Delta_{dd}^2}{\|\Omega_R\|^2}$
Average	$\frac{\pi\|\Omega_R\|}{\tau\omega_{ba}^2}\left(1+\frac{\|\Omega_R\|}{4\Delta_{dd}}\right)+\frac{\pi}{\tau\Delta_{dd}}\left(1+\frac{\Delta_{dd}}{\|\Omega_R\|}\right)$	$\frac{\|\Omega_R\|^2}{\omega_{ba}^2}+\frac{2\Delta_{dd}^2}{\|\Omega_R\|^2}$

and the vector $(1\ 0)^T$ represents $|b\rangle$. The last row in Table IV gives the gate error averaged over the possible input states. While a particular computation may weight certain input states more heavily than others the average gate error is indicative of the gate performance. The average error is minimized for

$$\Delta_{dd|\mathrm{opt}} \simeq \left(\frac{\pi|\Omega_R|^2}{4\tau}\right)^{1/3}\left(1+\frac{|\Omega_R|^2}{4\omega_{ba}^2}\right)^{1/3}$$

which determines the leading order contributions to the error as

$$E_{\mathrm{opt}} \simeq \frac{|\Omega_R|^2}{\omega_{ba}^2}+\frac{3}{2^{1/3}}\left(\frac{\pi}{\tau|\Omega_R|}\right)^{2/3}. \tag{37}$$

The optimum dipole-dipole shift, gate time $t_g=2\pi/|\Omega_R|+\pi/\Delta_{dd}|_{\mathrm{opt}}$, and gate error are shown in Fig. 7. We see that errors less than 10^{-2} are possible with Rabi frequencies of a few tens of MHz and a gate time of less than 1 μs. The corresponding optimum dipole-dipole shifts of order 1 MHz can be achieved at tens of microns of separation as we discuss in Sec. IV C.

Finally we note that the absolute minimum gate error occurs for $|\Omega_R|$ intermediate between ω_{ba} and $1/\tau$. Minimizing Eq. (37) with respect to $|\Omega_R|$ we find $|\Omega_R|_{\mathrm{opt}}=[\pi\omega_{ba}^3/(2^{1/2}\tau)]^{1/4}$ and a minimum error of $E|_{\mathrm{min}}=[2^{7/2}\pi/(\tau\omega_{ba})]^{1/2}$. For the parameters used in Fig. 7 we get $|\Omega_R|_{\mathrm{opt}}=2\pi\times 183$ MHz and $E|_{\mathrm{min}}=2.9\times 10^{-3}$.

Additional imperfections

There are two additional imperfections when working in the large Rabi frequency limit. The first of these is due to fluctuations in the distance between the atoms. For atomic separation large compared to the extent of the thermal motion the actual qubit separation will be $R+x_1+x_2$, with $\langle x_1^2\rangle=\langle x_2^2\rangle=(w_{f0}^2/4)(T_a/|U_m|)$. The variance of the interaction phase is easily shown to be $\Delta^2(\phi)=(9\pi^2/2)(w_{f0}^2/R^2)(T_a/|U_m|)$. Using this variance as a measure of the gate error gives $E=(1/4)\Delta^2(\phi)(1/4)=3.5\times 10^{-4}$ at $R=50$ μm. The final factor of 1/4 accounts for an averaging over the possible initial states. We see that at $R=50$ μm this error is small compared to the intrinsic gate error which dominates for $R\gtrsim 15$ μm.

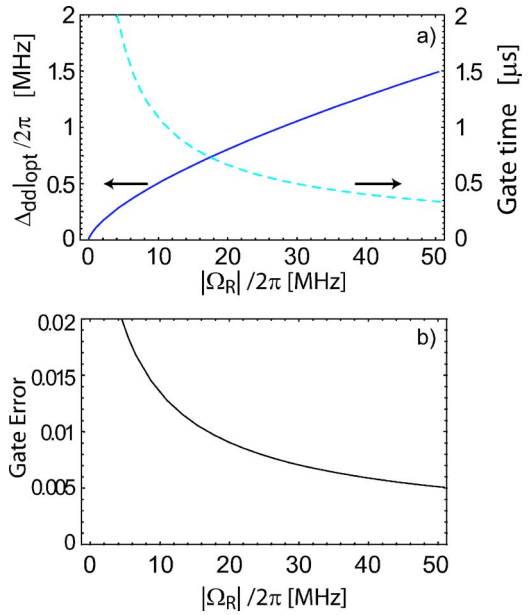

FIG. 7. (Color online) Two-qubit phase gate performance in the limit of large Rabi frequency: (a) optimum dipole-dipole shift and gate time, and (b) minimum achievable fidelity error. Calculations for $\tau=100$ μs and $\omega_{ba}=2\pi\times 6835$ MHz.

The second subsidiary imperfection is the presence of heating due to two-body forces when both atoms are excited to the Rydberg state. This effect could limit the number of gate operations before motional cooling is needed and lead to decoherence through undesired entanglement of the motional and spin states. The heating rate can be estimated simply as $P=Fv\sim F\omega_f w_{f0}$. Using $F=-dV_{dd}/dR$ for the two-body force we get a peak heating power of $P\sim 3\hbar\Delta_{dd}\omega_x w_{f0}/R$. Using $\Delta_{dd}=2\pi\times 1$ MHz and $R=50$ μm gives $P\sim 1.8$ μK/μs for our standard FORT parameters. We therefore expect a maximum of about 1 μK of heating when both atoms are initially in the state $|b\rangle$ which is coupled to the Rydberg states. Although the heating power will average to zero over many operations there is a finite probability for undesired motional entanglement. The spacing of the radial vibrational levels in temperature units is $\Delta E_{\mathrm{vib}}=\hbar\omega_x/k_B=1.9$ μK which is comparable to the peak heating value. On average there will be a reduced probability for a change of the vibrational state since the atoms spend proportionately more time near the turning points of the motion where the velocity is small.

The above errors due to fluctuations in the atomic separation and two-body forces are specific to gate operation in the large Rabi frequency limit. There is an additional error source that is common to both modes of gate operation, which is the presence of Doppler shifts of the Rydberg excitation beams due to atomic motion. For ground-state qubit rotations two-photon stimulated Raman transitions are essentially Doppler free for co-propagating beams, and the error given by Eq. (31) is insignificant. Two-photon excitation of Rydberg levels using 0.78 and 0.48 μm beams as indicated

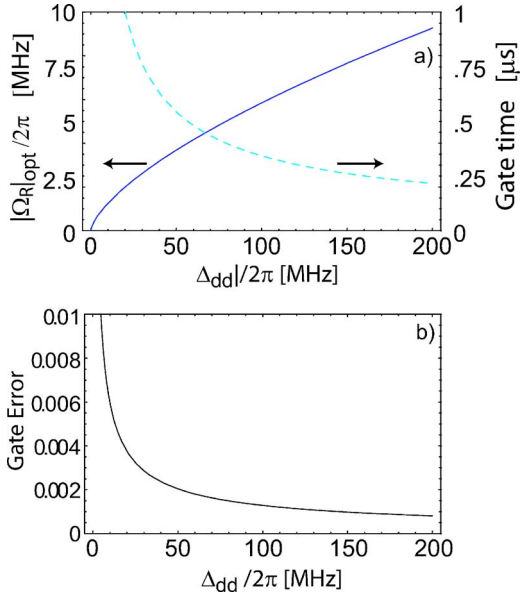

FIG. 8. (Color online) Two-qubit phase gate performance in the limit of large dipole-dipole shift: (a) optimum Rabi frequency and gate time, and (b) minimum achievable fidelity error. Calculations for $\tau=100$ μs and $\omega_{ba}=2\pi\times 6835$ MHz.

in Fig. 6 cannot be made Doppler free. For $T_a=50$ μK and $|\Omega_R|=2\pi\times 10$ MHz we find using Eq. (31), fidelity errors of 3.3×10^{-4} and 1.9×10^{-5} for co- and counter-propagating beams, respectively. These errors are significantly smaller than the intrinsic gate errors shown in Figs. 7 and 8.

B. Large dipole-dipole frequency shift

There is an alternative mode of operation of the phase gate that removes the dependence on variations in the interatomic separation and eliminates the two-body heating discussed above. This mode can be used for closely spaced atoms for which $\Delta_{dd}\gg|\Omega_R|$. In this limit the time scales have the ordering $1/\omega_{ba}\ll 1/\Delta_{dd}\ll 1/|\Omega_R|\ll\tau$. The protocol for a conditional phase gate is then [21] (ii) excite atom 1 (control atom) from $|b\rangle\rightarrow|r\rangle$ with a π pulse, (ii) excite atom 2 (target atom) from $|b\rangle\rightarrow|r\rangle\rightarrow|b\rangle$ with a 2π pulse, and (iii) transfer atom 1 back down from $|r\rangle\rightarrow|b\rangle$ with a π pulse. Note that in contrast to the protocol used in the large Rabi frqeuency limit we assume here that the atoms can be individually addressed.

The resulting idealized logic table is $|aa\rangle\rightarrow|aa\rangle$, $|ab\rangle\rightarrow|ab\rangle$, $|ba\rangle\rightarrow|ba\rangle$, $|bb\rangle\rightarrow-|bb\rangle$ which is an entangling phase gate. The gate errors are calculated using the same techniques as in Sec. IV A which results in the errors shown in Table V. The average error is minimized for

$$\Omega_{R\mathrm{opt}}\simeq\left(\frac{4\pi\Delta_{dd}^2}{\tau}\right)^{1/3}-\frac{4\pi\Delta_{dd}^2}{3\tau\omega_{ba}^2}$$

which determines the leading-order contributions to the error as

$$E_{\mathrm{opt}}\simeq\frac{3\pi^{2/3}}{2^{5/3}}\frac{1}{(\Delta_{dd}\tau)^{2/3}}\left(1+\frac{7\Delta_{dd}^2}{3\omega_{ba}^2}\right). \tag{38}$$

TABLE V. Leading contributions to the fidelity errors of a phase gate in the large dipole-dipole shift limit. See text for details.

Input state	Decoherence error	Rotation error
$\|aa\rangle$	$\frac{2\pi\|\Omega_R\|}{\tau\omega_{ba}^2}$	$\frac{2\|\Omega_R\|^2}{\omega_{ba}^2}$
$\|ab\rangle$	$\frac{\pi}{\tau\|\Omega_R\|}\left(1+\frac{\|\Omega_R\|^2}{\omega_{ba}^2}\right)$	$\frac{\|\Omega_R\|^2}{\omega_{ba}^2}$
$\|ba\rangle$	$\frac{\pi}{\tau\Delta_{dd}}+\frac{\pi}{\tau\|\Omega_R\|}\left(1+\frac{\|\Omega_R\|^2}{\omega_{ba}^2}\right)$	$\frac{\|\Omega_R\|^2}{2\omega_{ba}^2}$
$\|bb\rangle$	$\frac{\pi}{\tau}\left(\frac{2}{\|\Omega_R\|}+\frac{1}{\Delta_{dd}}\right)$	$\frac{\|\Omega_R\|^2}{2\Delta_{dd}^2}$
Average	$\frac{\pi}{\tau\|\Omega_R\|}\left(1+\frac{\|\Omega_R\|^2}{\omega_{ba}^2}\right)+\frac{\pi}{2\tau\Delta_{dd}}$	$\frac{\|\Omega_R\|^2}{8\Delta_{dd}^2}+\frac{7\|\Omega_R\|^2}{8\|\omega_{ba}\|^2}$

The optimum Rabi frequency, gate time $t_g=4\pi/|\Omega_R|_{\mathrm{opt}}|$, and gate error are shown in Fig. 8. We see that errors much less than 10^{-2} are possible with dipole-dipole shifts of a few tens of MHz and a gate time of less than 1 μs. This protocol appears more promising for achieving very small gate errors than the large Rabi frequency protocol, since it is easier to achieve very large dipole-dipole shifts than it is to achieve very large Rabi frequencies.

Finally we note that minimizing Eq. (38) with respect to Δ_{dd} we find $\Delta_{dd}|_{\mathrm{opt}}=\sqrt{3/14}\omega_{ba}$ and an absolute minimum error of $E|_{\mathrm{min}}=[1701\pi^2/(128\tau^2\omega_{ba}^2)]^{1/3}$. For the parameters used in Fig. 8 we get $\Delta_{dd}|_{\mathrm{opt}}=2\pi\times 3160$ MHz and $E|_{\mathrm{min}}=1.9\times10^{-4}$.

C. Dipole-dipole interaction strength

The long-range interactions between two Rydberg atoms are extremely strong and are the heart of the quantum computation scheme discussed in this paper. We consider here the Rydberg-Rydberg interactions in two limits: zero electric field, where the long-range $1/R^6$ van der Waals interactions are of primary importance, and in a hybridizing electric field, where the atoms attain a "permanent" dipole moment of magnitude n^2ea_0.

For S states, the van der Waals interaction is dominated by the near resonance between the states $nS+nS$ and $nP+(n-1)P$, as can be seen from Fig. 9. In the approximation that we neglect the contribution from other states, the Rydberg-Rydberg potential-energy curves are simply given by

$$V(R)=\frac{\delta}{2}+\sqrt{\frac{4U_3(R)^2}{3}+\frac{\delta^2}{4}}, \tag{39}$$

where $U_3(R)=e^2\langle 50S\|r\|50P\rangle\langle 50S\|r\|49P\rangle/(4\pi\epsilon_0R^3)=5.75\times10^3$ MHz μm$^3/R^3$ and the SS-PP energy defect is $\delta=E(49P)+E(50P)-2E(50S)=-3000$ MHz. At the 10-μm separations of interest here, $U_3\ll\delta$ so that

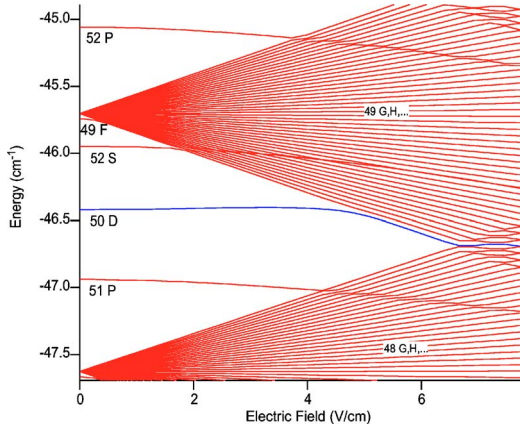

FIG. 9. (Color online) Stark map for states near $n=50$ for ^{87}Rb. At electric fields around 5–6 V/cm, the atom acquires a large permanent dipole moment, oriented in space along the applied field.

$$V(R) = -\frac{4U_3(R)^2}{3\delta}. \tag{40}$$

As can be seen from Fig. 10, the van der Waals potential for $50S$ is insufficient to allow for the MHz processing that is desired here.

van der Waals interactions between D states are dominated by the near resonance of $nD+nD$ and $(n+1)P+(n-1)F$. In general, the van der Waals interactions are of comparable strength when compared to the S states. Because of the degeneracy of the D levels, however, it can be shown that U_3 vanishes for one each of the $^3\Sigma_u^+$ and $^1\Sigma_g^+$ molecular states [57]. Thus there is no blockade at zero field for these states.

The scaling of the van der Waals interaction with n is very rapid, $V \propto n^{11}$. For $n=100$, $V(10\ \mu\text{m}) \sim 50$ MHz. While this is sufficient for a conditional phase gate (see Fig. 8) we can considerably enhance the interaction strength by applying a dc field. Thus we now consider the long-range interactions in the presence of an applied electric field.

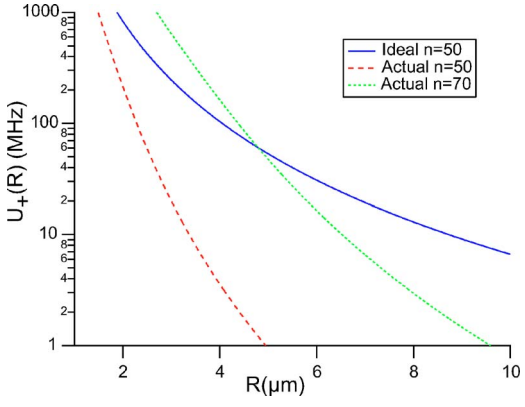

FIG. 10. (Color online) Isotropic dipole-dipole interaction for excitation to the Rb $50S$ state. The energy defect between the $50S+50S$ and $49P+50P$ states significantly reduces the interaction as compared to the ideal degenerate case. Going to larger n partially compensates for the nonzero energy defect.

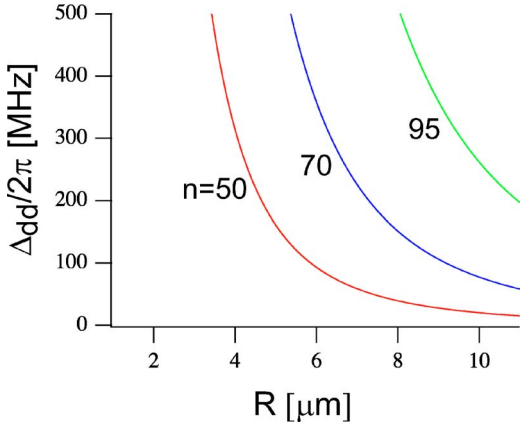

FIG. 11. (Color online) Dipole-dipole interaction strengths as a function of interatomic distance for various principal quantum numbers.

There are two primary ways to enhance the Rydberg-Rydberg interaction using an applied electric field. The first is to use the electric-field dependence of the state energies to bring the energy defect δ to zero, in which case $V(R) \approx 2U_3(R)/\sqrt{3}$. This would produce an extremely strong isotropic interaction of maximum strength, for example $n=95$ gives a frequency shift at 10-μm separation of 160 MHz. However, inspection of Fig. 9 shows that the P states tune the wrong way in an electric field, increasing rather than decreasing δ. For D states there remains the problem of zero dipole-dipole interactions for some molecular symmetries.

The second way to adjust the Rydberg-Rydberg interactions is to use a large enough field to strongly mix states of different L. In this case the atom acquires a field-independent dipole moment, as suggested for example by the linear field dependence of the $50D$ state at electric fields between 5 and 6 V/cm. In this case the Rydberg-Rydberg interaction is strong but anisotropic and we have the dipole-dipole interaction of Eq. (35),

$$V_{dd}(R) = \hbar\Delta_{dd}(R) = \frac{\mu^2}{4\pi\epsilon_0 R^3}(1-3\cos^2\theta), \tag{41}$$

where θ is the angle between the interatomic axis and the electric field.

In the proposed geometry for the quantum computer, the electric fields can be aligned to $\theta=0$ for maximum interaction strength. The electric dipole moment is on the order of $n^2 e a_0$, giving a dipole-dipole interaction of comparable size as the zero field case with $\delta=0$. We have numerically estimated the dipole moments for the field-mixed D states, and obtain for example $\mu=3300 e a_0$ for $n=50$. The resulting interaction strengths as a function of distance are shown in Fig. 11. We see that interaction frequencies in excess of 100 MHz can be achieved for $R=8$ μm at $n=70$ and well beyond $R=10$ μm at $n=95$. Thus the dipole-dipole interaction strength needed to optimize the phase gate, as shown in Fig. 8, can be achieved for qubit separations that are optically resolvable. It has been pointed out [58] that n should not be too large in order to avoid collisions between the valence electrons of neighboring Rydberg atoms. For $R=8$ μm this implies that n

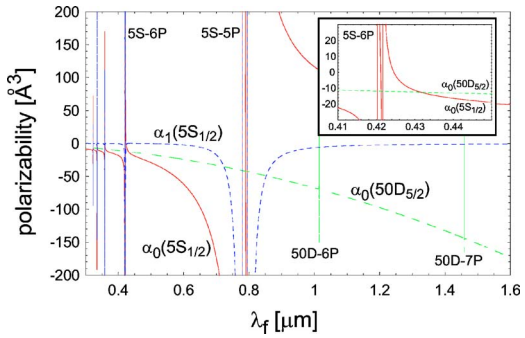

FIG. 12. (Color online) Polarizability of the $5S_{1/2}$ and $50D_{5/2}$ states. The inset shows the behavior near the $5S$-$6P$ transition.

should be less than about 100. Although $n=100$ is sufficient for the geometry considered here, it is also true that in the large dipole-dipole shift limit discussed above this limitation is not needed as only one atom at a time is excited to a Rydberg level.

D. Balancing the ground- and excited-state polarizabilities

The implementation of the two-qubit conditional gate described so far has an inherent flaw that stems from the need to make real transitions to Rydberg levels. The atoms are confined in attractive optical potential wells since the ground-state polarizability is positive for light tuned to the red of the first Rb resonance lines. However, for the same red detuned trapping laser, the high-lying Rydberg levels have a negative polarizability that provides a repulsive potential. Excitation of an atom to the repulsive Rydberg state during a gate cycle leads to heating and decoherence through entanglement of the spin and motional states. Looking at Fig. 12 we see that for $\lambda_f=1.06$ μm the $50D_{5/2}$ Rydberg level has a polarizability of $\alpha_0(50D_{5/2})=-77$ Å^3. This polarizability is about 95% of the free-electron polarizability of $-e^2/m_e\omega_f^2$, with m_e the electron mass. This implies that the Rydberg polarizability is only weakly dependent on the principal quantum number n for large n, so the discussion given here for the case of the $50D_{5/2}$ level is applicable to any of the highly excited states.

When the Rydberg state sees a repulsive potential the heating is minimized by turning off the trapping laser during the gate operation. For atomic temperatures large compared to the trap vibrational energy the motion is quasiclassical and the average heating per gate cycle of duration τ is $\langle \Delta U\rangle = T_a 1/2(\omega\tau)^2$, where ω is the radial trap vibration frequency. For $\tau=0.5$ μs and $\omega=2\pi\times 39$ kHz we get $\langle \Delta U\rangle/T_a=7.5\times 10^{-3}$. This heating rate is about 5 times larger than that due to the ac Stark shifts of the Raman lasers discussed in Sec. III B, and implies that several hundred operations can be performed before there is significant heating of the atomic motion.

The heating can be eliminated by choosing a FORT laser wavelength that gives equal polarizability for the ground and Rydberg states. Referring to Fig. 12, one possibility is to tune the FORT laser to the blue side of the $50D$-$6P$ transition where the Rydberg level acquires a positive polarizability. The scalar polarizability of the Rydberg level is given by

$$\alpha_0(nD_{5/2}) = -\frac{2}{3\hbar}\frac{1}{2J+1}\sum_{\gamma' J'}\frac{\omega_{\gamma' J',\gamma J}}{\omega_{\gamma' J',\gamma J}^2-\omega_f^2}|\langle \gamma' J'\|\hat{D}\|\gamma J\rangle|^2, \tag{42}$$

where $\hat{D}$ is the electric dipole operator and $\hbar\omega_{\gamma' J',\gamma J}=E_{\gamma' J'}-E_{\gamma J}$. Away from the resonance the polarizability changes slowly with ω_f and for the $|50D_{5/2}\rangle$ level it is $\bar{\alpha}_0(50D_{3/2})\simeq -69$ Å^3. When ω_f is near resonant with the $|nD_{5/2}\rangle\leftrightarrow|6P_{3/2}\rangle$ transition the polarizability is the sum of the background value $\bar{\alpha}_0$ plus the resonant contribution to the sum. Using Coulomb wave functions for $n=50$ we find $\langle 50D_{5/2}\|\hat{D}\|6P_{3/2}\rangle=0.059ea_0$ so that a rough estimate for the detuning condition at which the polarizabilities are equal is

$$\Delta_f = \frac{1}{3\hbar}\frac{1}{2J+1}\frac{|\langle 50D_{5/2}\|\hat{D}\|6P_{3/2}\rangle|^2}{\alpha_0(5S_{1/2})-\bar{\alpha}_0(50D_{5/2})} = 2\pi\times 945 \text{ MHz}. \tag{43}$$

Unfortunately there is a penalty associated with balancing the polarizabilities in this way since there is a probability for the gate operation to end with the atom having finite amplitude to be in the $|6P_{3/2}\rangle$ level which lies outside the computational basis. The Rabi frequency for this transition (starting from $m_J=3/2$) is given by $|\Omega_f| = [\mathcal{E}_f/(\hbar\sqrt{15})]\langle 50D_{5/2}\|\hat{D}\|6P_{3/2}\rangle$ and the probability for population transfer to the $|6P_{3/2}\rangle$ state at the end of a Rydberg operation is bounded by $P_{\max}=|\Omega_f|^2/(|\Omega_f|^2+\Delta_f^2)$. For a trap depth of 1 mK we find $|\Omega_f|=2\pi\times 210$ MHz and $P_{\max}=0.16$. This upper bound assumes that the ratio of the gate time and the spontaneous lifetime of the $6P$ level is not large, otherwise there is an additional loss mechanism due to decay out of the $6P$ level.

This decoherence probability is roughly proportional to the FORT laser intensity and can be reduced by working with a shallower FORT trap. This suggests that atoms be loaded into 1-mK-deep traps where they can be cooled to sub Doppler temperatures with standard methods, followed by adiabatic reduction of the trap depth before performing logical operations. With $T_a=5$ μK and $|U_m|=100$ μK the atom localization and motional errors will be the same as considered in the rest of this paper, while the decoherence probability per Rydberg operation will be bounded by $P_{\max}=0.016$.

While we expect this to be a viable approach for initial experiments it can be readily shown that the decoherence probability with polarizability balancing of a nD Rydberg level scales proportional to $1/|\langle nD_{5/2}\|\hat{D}\|6P_{3/2}\rangle|^2$. Since $|\langle nD_{5/2}\|\hat{D}\|6P_{3/2}\rangle|^2\sim 1/n^3$ the leakage problem scales as n^3 and the technique is most useful for low-lying Rydberg states that have large transition dipole moments with the $6P$ level.

An alternative solution is to choose a FORT wavelength such that the ground state acquires a negative polarizability which coincides with that of the Rydberg level. In this situation the optical potential is negative so the atom is trapped at a local minimum of the intensity. This approach has a number of advantages since for an intensity profile of the

form $I=I_0(1-e^{-2r^2/w_{f0}^2})$ the time averaged trapping intensity at the position of the atom is $T_a/|U_m|$ times smaller than it would be for an attractive potential of the same depth. This increases the T_1 and T_2 times in rows 2, 3, and 6 of Table I associated with photon scattering and motional ac Stark shifts by the same factor. It was pointed out by Safronova *et al.* [59] that the polarizabilities can be balanced in this way by tuning the trapping laser between the D lines. For ^{87}Rb the balancing point is at $\lambda_f \simeq 0.79$ μm. However, the vector polarizability at this point has a very large value of $\alpha_1 \simeq 3600$ Å^3 which would lead to a T_1 due to inelastic scattering [see Eq. (12)] of about 1 ms for the parameters of Table I, which is unacceptably short.

A more favorable alternative is to use a FORT wavelength of $\lambda_f \simeq 0.431$ μm which gives equal polarizabilities of $\alpha_0 \simeq -12.5$ Å^3, as shown in the inset to Fig. 12. At this wavelength $\alpha_1 \simeq -0.01$ Å^3 which gives an inelastic scattering T_1 that is longer than any other time scale in Table I. The only drawbacks of this solution are technical, not fundamental. There is additional experimental complexity associated with creating optical beams with local intensity minima, as well as the need for a medium power laser in the blue. Recent developments in solid-state laser sources and parametric frequency convertors render the latter requirement readily solvable.

E. Rydberg state radiative lifetimes

The lifetimes of highly excited Rydberg nl states are affected strongly by background blackbody radiation. If the 0-K lifetime is $\tau_{nl}^{(0)}$ the finite temperature lifetime can be written as

$$\frac{1}{\tau_{nL}} = \frac{1}{\tau_{nL}^{(0)}} + \frac{1}{\tau_{nL}^{(\mathrm{bb})}}, \tag{44}$$

where $\tau_{nL}^{(\mathrm{bb})}$ is the finite temperature blackbody contribution. The 0-K radiative lifetime can be calculated by summing over transition rates or approximated by the expression [60]

$$\tau_{nL}^{(0)} = \tau_L^{(0)}(n^*)^{\alpha_L}. \tag{45}$$

For all the alkalis $\alpha_L \simeq 3$. Parameters for Rb are $\alpha_S=2.94$, $\alpha_P=3.02$, $\alpha_D=2.85$, $\alpha_F=2.95$, and $\tau_S^{(0)}=1.43$, $\tau_P^{(0)}=2.76$, $\tau_D^{(0)}=2.09$, and $\tau_F^{(0)}=0.76$ in units of ns.

For large n the blackbody rate can be written approximately as [61]

$$\frac{1}{\tau_{nL}^{(\mathrm{bb})}} = \frac{4\alpha^3 k_B T}{3\hbar n^2}, \tag{46}$$

where α is the fine-structure constant. Equation (46) includes transitions to continuum states so that it accounts for blackbody induced photoionization. Figure 13 shows the radiative lifetime τ_{nL} for n up to 100 and several l states. We see that for $n \gtrsim 65$ the S,P,D, and F states have lifetimes greater than 0.1 ms at room temperature.

F. FORT trap induced photoionization

Highly excited states are also unstable against photoionization from the intense trapping light. Since the Rydberg electron is nearly free, and the photoionization is far above threshold, the photoionization cross sections are small. We have estimated the photoionization rate of high Rydberg states by calculating the cross section using Rydberg and continuum wave functions.

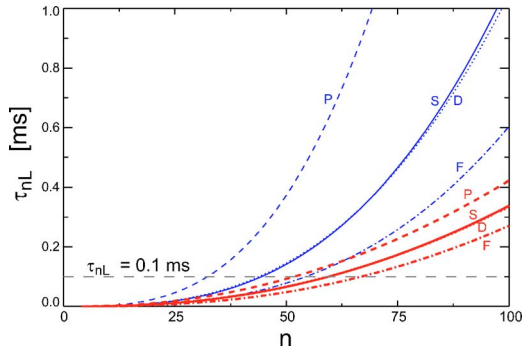

FIG. 13. (Color online) Excited-state lifetime due to radiative decay for $T=0$ (blue, thin lines) and $T=300$ K (red, thick lines) for S,P,D, and F states of Rb.

The cross section is given by [61]

$$\sigma = 2\pi^2 \frac{\hbar e^2}{mc} \left.\frac{df}{dE}\right|_{E_c}, \tag{47}$$

where f is the oscillator strength and $E_c=\hbar\omega+E_r$ the energy of the continuum electron produced by the photon of frequency ω from the Rydberg state of energy E_r. The oscillator strength distribution is

$$\frac{df}{dE} = \sum_L \frac{2m\omega L_>}{3\hbar(2L_r+1)} \left| \int \Psi_r(r) r \phi_{L,E}(r) dr \right|^2, \tag{48}$$

where $L_>$ is the larger of L_r and L and the continuum wave function is normalized per unit energy

$$\phi_{L,E}(r) \overset{r\to\infty}{\sim} \sqrt{\frac{2m}{\pi\hbar^2 k}} \sin(kr + \delta_{L,E}). \tag{49}$$

We have used two methods to detemine the bound and continuum wave functions. In the first we use quantum defect theory [62] to find the Coulomb wave functions and phase shifts $\delta_{L,E}$. The second method uses the L-dependent model potentials of Marinescu *et al.* [63], with values slightly adjusted to give the proper quantum defects of the Rydberg states. The Numerov method was then used to find $\phi_{L,E}$. Numerical results for the two approaches agree within a factor of about 2 for the range of n discussed here. The discussion and Fig. 14 give the results obtained using the Marinescu potential.

The $n=50$ photoionization cross sections are shown as a function of L in Fig. 14. The photoionization cross section for the S state is much smaller than $L>0$ states due to the $\pi/2$ phase shift between the S and P wave functions [61]. The cross sections increase dramatically for the P and D states before slowly decreasing with further increases in L. While the 50S cross sections are very small, the 100× larger cross section for the higher L levels implies that the photoionization rate for the S states will depend sensitively on

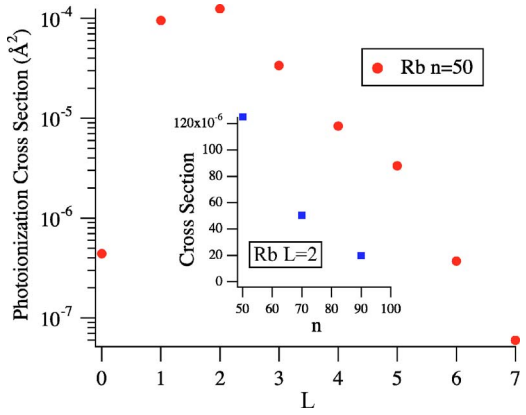

FIG. 14. (Color online) Photoionization cross section vs ejected electron energy, for the Rb 50*S* Rydberg state with $\lambda_f = 1.01$ μm.

mixing with the *P* levels due to external fields. Thus the photoionization cross sections may be as large as 10^{-20} cm^2, or as high as $\gamma_{\rm pi} = 31\,000/\rm s$ for a 1-mK trap depth.

The photoionization cross sections decrease with *n*, a factor of 6 going from $n=50$ to $n=90$ as shown in the inset to Fig. 14. Thus at $n=90$ we get a minimum lifetime of $\tau_{\rm pi} \sim 190$ μs for the *P* and *D* states and substantially longer for the other *L* states. Taking into account the blackbody lifetime calculated in the previous section we conclude that the Rydberg lifetime will exceed 100 μs for $n \gtrsim 80$. This validates the gate fidelity estimates discussed in Secs. IV A and IV B. Since the photoionization rate scales linearly with the trap depth even better performance is possible by further cooling of the atomic motion and a corresponding reduction of the trap depth, or by use of a blue detuned FORT laser as discussed in Sec. IV D.

V. DISCUSSION

In this paper we have presented a detailed analysis of quantum logic using neutral atoms localized in optical traps. Two-photon Raman transitions are used for single-qubit gates, dipole-dipole interactions of Rydberg states provide a two-qubit conditional phase gate, and detection of resonance fluorescence is used for state measurement. We have concentrated on an implementation of neutral atom gates that should be feasible with currently available experimental methods and laser sources. The T_1 and T_2 coherence times for qubit storage, and error estimates for single-qubit gates are summarized in Tables I and II. The intrinsic two-qubit gate errors are shown in Figs. 7 and 8. The analysis supports the feasibility of MHz rate logical operations with intrinsic errors $O(10^{-4})$ for single-qubit operations, $O(10^{-3})$ for two-qubit gates, and state measurements in less than 100 μs with $O(10^{-3})$ measurement error. We show that coherence times of at least several seconds are possible in red-detuned attractive optical traps. Taken together these numbers suggest an attractive framework for experimental studies of quantum logic with neutral atoms.

It should be emphasized that the Rydberg gate approach does not rely on cooling the atoms to the motional ground state. While ground-state cooling has been demonstrated in optical traps, and lower atomic temperatures will lengthen coherence times and reduce some of the gate errors, the difficulty of maintaining the atoms in the motional ground state in the presence of heating mechanisms should not be overlooked. Our assumption of $T_a = 50$ μK does not require complex cooling schemes, and implies that $O(10^3)$ single-qubit logical operations can be performed without significant reduction in fidelity due to motional heating.

As discussed in Sec. IV D the differential polarizability of the ground and Rydberg states in a red-detuned FORT will lead to substantial heating or loss of coherence. While initial experiments are viable in red-detuned FORTs our analysis suggests that a blue FORT where the atoms are trapped at a local minimum of the intensity will ultimately be necessary to realize the full potential of this scheme. The blue FORT will also substantially improve the coherence times for qubit storage, and to a lesser extent the Rydberg state lifetime.

Extending the two-qubit approach described here to a large number of qubits will involve solving challenges related to loading and addressing of multiple sites. The Rydberg gate approach does appear intrinsically well suited for implementation in a two-dimensional array, including error correction blocks. The large dipole-dipole shift limit can be used for gates between neighboring sites, while the large Rabi frequency limit which works at longer range may allow non-nearest neighbors to be coupled. Figure 7 shows that in the limit of large Rabi frqeuency, gate errors less than 10^{-2} are possible with dipole-dipole coupling strengths of only 1 MHz. For Rydberg levels with $n=70$ we can achieve a coupling strength of 1 MHz at a separation of about 40 μm. With a 8-μm qubit spacing this suggests the possibility of coupling blocks of 25 or more qubits without physical motion. By taking advantage of the directional properties of the dipole-dipole interaction described by Eq. (35) it is possible to perform row parallel operations between pairs of qubits with strongly suppressed crosstalk. While there are many appealing features of the approach studied here we emphasize that the extent to which it will prove possible to perform arbitrarily large, scalable quantum computations remains an open question that will require a great deal of further theoretical and experimental studies.

ACKNOWLEDGMENTS

We thank the members of the Rydberg atom quantum computing group at Madison for helpful discussions. This work was supported by the U. S. Army Research Office under Contract No. DAAD19-02-1-0083, and NSF Grant Nos. EIA-0218341 and PHY-0205236.

APPENDIX: RAMAN TRANSITIONS DUE TO IMPERFECT POLARIZATION

We account for imperfect polarization of the Raman beams by putting $\boldsymbol{\epsilon}_1 = (\mathbf{e}_+ + \epsilon_{1-}\mathbf{e}_- + \epsilon_{10}\mathbf{e}_0)/(1+\epsilon_{1-}^2+\epsilon_{10}^2)^{1/2}$ and $\boldsymbol{\epsilon}_2 = (\mathbf{e}_+ + \epsilon_{2-}\mathbf{e}_- + \epsilon_{20}\mathbf{e}_0)/(1+\epsilon_{2-}^2+\epsilon_{20}^2)^{1/2}$. Referring to Fig. 4 and limiting ourselves to transition amplitudes that are linear in the small parameters $\boldsymbol{\epsilon}$ we must account for the following undesired transitions starting from $|a\rangle = |10\rangle$:

$$|a\rangle \to |1-1\rangle \quad \epsilon_{10}(\mathcal{E}_1\mathbf{e}_0)(\mathcal{E}_1\mathbf{e}_+)^* + \epsilon_{20}(\mathcal{E}_2\mathbf{e}_0)(\mathcal{E}_2\mathbf{e}_+)^*,$$

$$|a\rangle \to |11\rangle \quad \epsilon_{10}^*(\mathcal{E}_1\mathbf{e}_+)(\mathcal{E}_1\mathbf{e}_0)^* + \epsilon_{20}^*(\mathcal{E}_2\mathbf{e}_+)(\mathcal{E}_2\mathbf{e}_0)^*,$$

$$|a\rangle \to |2-2\rangle \quad \epsilon_{1-}(\mathcal{E}_1\mathbf{e}_-)(\mathcal{E}_2\mathbf{e}_+)^*,$$

$$|a\rangle \to |2-1\rangle \quad \epsilon_{10}(\mathcal{E}_1\mathbf{e}_0)(\mathcal{E}_2\mathbf{e}_+)^*,$$

$$|a\rangle \to |21\rangle \quad \epsilon_{20}^*(\mathcal{E}_1\mathbf{e}_+)(\mathcal{E}_2\mathbf{e}_0)^*,$$

$$|a\rangle \to |22\rangle \quad \epsilon_{2-}^*(\mathcal{E}_1\mathbf{e}_+)(\mathcal{E}_2\mathbf{e}_-)^*, \tag{A1}$$

and the following transitions starting from $|b\rangle=|20\rangle$:

$$|b\rangle \to |1-1\rangle \quad \epsilon_{20}(\mathcal{E}_2\mathbf{e}_0)(\mathcal{E}_1\mathbf{e}_+)^*,$$

$$|b\rangle \to |11\rangle \quad \epsilon_{10}^*(\mathcal{E}_2\mathbf{e}_+)(\mathcal{E}_1\mathbf{e}_0)^*,$$

$$|b\rangle \to |2-2\rangle \quad \epsilon_{1-}(\mathcal{E}_1\mathbf{e}_-)(\mathcal{E}_1\mathbf{e}_+)^* + \epsilon_{2-}(\mathcal{E}_2\mathbf{e}_-)(\mathcal{E}_2\mathbf{e}_+)^*,$$

$$|b\rangle \to |2-1\rangle \quad \epsilon_{10}(\mathcal{E}_1\mathbf{e}_0)(\mathcal{E}_1\mathbf{e}_+)^* + \epsilon_{20}(\mathcal{E}_2\mathbf{e}_0)(\mathcal{E}_2\mathbf{e}_+)^*,$$

$$|b\rangle \to |21\rangle \quad \epsilon_{10}^*(\mathcal{E}_1\mathbf{e}_+)(\mathcal{E}_1\mathbf{e}_0)^* + \epsilon_{20}^*(\mathcal{E}_2\mathbf{e}_+)(\mathcal{E}_2\mathbf{e}_0)^*,$$

$$|b\rangle \to |22\rangle \quad \epsilon_{1-}^*(\mathcal{E}_1\mathbf{e}_+)(\mathcal{E}_1\mathbf{e}_-)^* + \epsilon_{2-}^*(\mathcal{E}_2\mathbf{e}_+)(\mathcal{E}_2\mathbf{e}_-)^*. \tag{A2}$$

We have labeled the kets as $|F,m_F\rangle$ and the factors on the

TABLE VI. Transition amplitudes out of the computational basis due to imperfect optical polarization. The effective Raman frequencies are given by $\Omega_R=[2e^2R_{5S,5P_{1/2}}^2/(\epsilon_0c\hbar^2)](K/72)I$, with I the intensity of each Raman beam. The last column shows the amplitude of the leakage state for a π pulse on the $|a\rangle\to|b\rangle$ (or $|b\rangle\to|a\rangle$) transition, evaluated using Eq. (23) with $I=100$ μW and $\Delta_{11}/2\pi=-100$ GHz such that $|\Omega_R(|a\rangle\to|b\rangle)|/2\pi=4.6$ MHz.

Transition	K	Transition Stark shift (MHz)	Transition amplitude
$\|a\rangle\to\|1-1\rangle$	$-\frac{2\epsilon_{10}}{(\Delta_{11}-\Delta_e)}-\frac{2\epsilon_{20}}{(\Delta_{11}-\Delta_e-\omega_{ba})}$	−2.41	-4.1×10^{-3}
$\|a\rangle\to\|11\rangle$	$\epsilon_{10}^*\left(\frac{1}{\Delta_{11}}-\frac{3}{\Delta_{11}-\Delta_e}\right)+\epsilon_{20}^*\left(\frac{1}{\Delta_{11}-\omega_{ba}}-\frac{3}{\Delta_{11}-\Delta_e-\omega_{ba}}\right)$	2.42	-4.1×10^{-3}
$\|a\rangle\to\|2-2\rangle$	$-\sqrt{6}\epsilon_{1-}\left(\frac{1}{\Delta_{11}}-\frac{1}{\Delta_{11}-\Delta_e}\right)$	−4.79	1.3×10^{-5}
$\|a\rangle\to\|2-1\rangle$	$\frac{2\sqrt{3}\epsilon_{10}}{\Delta_{11}-\Delta_e}$	−2.39	3.4×10^{-3}
$\|a\rangle\to\|21\rangle$	$-\sqrt{3}\epsilon_{20}^*\left(\frac{1}{\Delta_{11}}+\frac{1}{\Delta_{11}-\Delta_e}\right)$	2.38	-3.4×10^{-3}
$\|a\rangle\to\|22\rangle$	$\sqrt{6}\epsilon_{2-}^*\left(\frac{1}{\Delta_{11}}-\frac{1}{\Delta_{11}-\Delta_e}\right)$	4.75	-1.4×10^{-5}
$\|b\rangle\to\|1-1\rangle$	$-\frac{2\epsilon_{20}}{\Delta_{11}}$	−2.41	-1.9×10^{-3}
$\|b\rangle\to\|11\rangle$	$-\epsilon_{10}^*\left(\frac{1}{\Delta_{11}}-\frac{3}{\Delta_{11}-\Delta_e}\right)$	2.42	2.0×10^{-3}
$\|b\rangle\to\|2-2\rangle$	$-\sqrt{6}\epsilon_{1-}\left(\frac{1}{\Delta_{11}+\omega_{ba}}-\frac{1}{\Delta_{11}-\Delta_e+\omega_{ba}}\right)-\sqrt{6}\epsilon_{2-}\left(\frac{1}{\Delta_{11}}-\frac{1}{\Delta_{11}-\Delta_e}\right)$	−4.79	2.5×10^{-5}
$\|b\rangle\to\|2-1\rangle$	$\frac{2\sqrt{3}\epsilon_{10}}{\Delta_{11}+\omega_{ba}}+\frac{2\sqrt{3}\epsilon_{20}}{\Delta_{11}}$	−2.39	6.5×10^{-3}
$\|b\rangle\to\|21\rangle$	$\sqrt{3}\epsilon_{10}^*\left(\frac{1}{\Delta_{11}+\omega_{ba}}+\frac{1}{\Delta_{11}-\Delta_e+\omega_{ba}}\right)+\sqrt{3}\epsilon_{20}^*\left(\frac{1}{\Delta_{11}}+\frac{1}{\Delta_{11}-\Delta_e}\right)$	2.38	6.6×10^{-3}
$\|b\rangle\to\|22\rangle$	$-\sqrt{6}\epsilon_{1-}^*\left(\frac{1}{\Delta_{11}+\omega_{ba}}-\frac{1}{\Delta_{11}-\Delta_e+\omega_{ba}}\right)-\sqrt{6}\epsilon_{2-}^*\left(\frac{1}{\Delta_{11}}-\frac{1}{\Delta_{11}-\Delta_e}\right)$	4.75	2.5×10^{-5}

right indicate the participating fields and polarizations. The Clebsch-Gordan factors and detunings associated with these transitions are different than those that apply for the desired $|a\rangle \rightarrow |b\rangle$ transition. We will assume that the fields are in two-photon resonance for the $|a\rangle \rightarrow |b\rangle$ transition accounting for the ac Stark shifts given in Table III. The Rabi frequencies normalized to that of the desired transition are given in Table VI which shows the transition amplitude for excitation of an undesired state with parameters that give a π pulse on the desired transition.

[1] M. A. Nielsen and I. L. Chuang, *Quantum Computation and Quantum Information* (Cambridge University Press, Cambridge, England, 2000);A. Steane, Rep. Prog. Phys. **61**, 117 (1998); *The Physics of Quantum Information*, edited by D. Bouwmeester, A. Ekert, and A. Zeilinger (Springer, Berlin, 2000).

[2] Q. A. Turchette, C. J. Hood, W. Lange, H. Mabuchi, and H. J. Kimble, Phys. Rev. Lett. **75**, 4710 (1995).

[3] C. Monroe, D. M. Meekhof, B. E. King, W. M. Itano, and D. J. Wineland, Phys. Rev. Lett. **75**, 4714 (1995).

[4] C. A. Sackett, D. Kielpinski, B. E. King, C. Langer, V. Meyer, C. J. Myatt, M. Rowe, Q. A. Turchette, W. M. Itano, D. J. Wineland, and C. Monroe, Nature (London) **404**, 256 (2000).

[5] P. G. Kwiat, A. J. Berglund, J. B. Altepeter, and A. G. White, Science **290**, 498 (2000).

[6] I. L. Chuang, L. M. K. Vandersypen, X. Zhou, D. W. Leung, and S. Lloyd, Nature (London) **393**, 143 (1998).

[7] E. Knill, R. Laflamme, R. Martinez, and C. Negrevergne, Phys. Rev. Lett. **86**, 5811 (2001).

[8] J. Chiaverini, D. Leibfried, T. Schaetz, M. D. Barrett, R. B. Blakestad, J. Britton, W. M. Itano, J. D. Jost, E. Knill, C. Langer, R. Ozeri, and D. J. Wineland, Nature (London) **432**, 602 (2004).

[9] D. Leibfried, R. Blatt, C. Monroe, and D. Wineland, Rev. Mod. Phys. **75**, 281 (2003).

[10] L. M. K. Vandersypen, M. Steffen, G. Breyta, C. S. Yannoni, M. H. Sherwood, and I. L. Chuang, Nature (London) **414**, 883 (2001).

[11] R. Laflamme, D. Cory, C. Negrevergne, and L. Viola, Quantum Inf. Comput. **2**, 166 (2002).

[12] J. I. Cirac and P. Zoller, Phys. Rev. Lett. **74**, 4091 (1995).

[13] D. J. Wineland, C. Monroe, W. M. Itano, D. Leibfried, B. E. King, and D. M. Meekhof, J. Res. Natl. Inst. Stand. Technol. **103**, 259 (1998).

[14] F. Schmidt-Kaler, H. Häffner, M. Riebe, S. Gulde, G. P. T. Lancaster, T. Deuschle, C. Becher, C. F. Roos, J. Eschner, and R. Blatt, Nature (London) **422**, 408 (2003).

[15] G. K. Brennen, C. M. Caves, P. S. Jessen, and I. H. Deutsch, Phys. Rev. Lett. **82**, 1060 (1999).

[16] D. Jaksch, H.-J. Briegel, J. I. Cirac, C. W. Gardiner, and P. Zoller, Phys. Rev. Lett. **82**, 1975 (1999).

[17] I. H. Deutsch, G. K. Brennen, and P. S. Jessen, Fortschr. Phys. **48**, 925 (2000).

[18] T. Calarco, H.-J. Briegel, D. Jaksch, J. I. Cirac, and P. Zoller, Fortschr. Phys. **48**, 945 (2000).

[19] A. M. Steane and D. M. Lucas, Fortschr. Phys. **48**, 839 (2000).

[20] J. Mompart, K. Eckert, W. Ertmer, G. Birkl, and M. Lewenstein, Phys. Rev. Lett. **90**, 147901 (2003).

[21] D. Jaksch, J. I. Cirac, P. Zoller, S. L. Rolston, R. Côté, and M. D. Lukin, Phys. Rev. Lett. **85**, 2208 (2000).

[22] I. E. Protsenko, G. Reymond, N. Schlosser, and P. Grangier, Phys. Rev. A **65**, 052301 (2002).

[23] M. Greiner, O. Mandel, T. Esslinger, T. W. Hänsch, and I. Bloch, Nature (London) **415**, 39 (2002).

[24] S. Peil, J. V. Porto, B. L. Tolra, J. M. Obrecht, B. E. King, M. Subbotin, S. L. Rolston, and W. D. Phillips, Phys. Rev. A **67**, 051603(R) (2003).

[25] J. Vala, A. V. Thapliyal, S. Myrgren, U. Vazirani, D. S. Weiss, and K. B. Whaley, Phys. Rev. A **71**, 032324 (2005).

[26] P. Rabl, A. J. Daley, P. O. Fedichev, J. I. Cirac, and P. Zoller, Phys. Rev. Lett. **91**, 110403 (2003).

[27] R. Scheunemann, F. S. Cataliotti, T. W. Hänsch, and M. Weitz, Phys. Rev. A **62**, 051801(R) (2000).

[28] R. Dumke, M. Volk, T. Müther, F. B. J. Buchkremer, G. Birkl, and W. Ertmer, Phys. Rev. Lett. **89**, 097903 (2002).

[29] M. Saffman and T. G. Walker, Phys. Rev. A **66**, 065403 (2002).

[30] M. Saffman, Opt. Lett. **29**, 1016 (2004).

[31] D. Frese, B. Ueberholz, S. Kuhr, W. Alt, D. Schrader, V. Gomer, and D. Meschede, Phys. Rev. Lett. **85**, 3777 (2000).

[32] N. Schlosser, G. Reymond, I. Protsenko, and P. Grangier, Nature (London) **411**, 1024 (2001).

[33] S. Chu, J. E. Bjorkholm, A. Ashkin, and A. Cable, Phys. Rev. Lett. **57**, 314 (1986).

[34] J. D. Miller, R. A. Cline, and D. J. Heinzen, Phys. Rev. A **47**, R4567 (1993).

[35] K. D. Bonin and V. V. Kresin, *Electric-dipole Polarizabilities of Atoms, Molecules and Clusters* (World Scientific, Singapore, 1997).

[36] S. Bali, K. M. OHara, M. E. Gehm, S. R. Granade, and J. E. Thomas, Phys. Rev. A **60**, R29 (1999).

[37] T. A. Savard, K. M. O'Hara, and J. E. Thomas, Phys. Rev. A **56**, R1095 (1997).

[38] L. W. Anderson, Nuovo Cimento **22**, 936 (1961).

[39] M. V. Romalis and E. N. Fortson, Phys. Rev. A **59**, 4547 (1999).

[40] C. Chin, V. Leiber, V. Vuletić, A. J. Kerman, and S. Chu, Phys. Rev. A **63**, 033401 (2001).

[41] A. Kaplan, M. F. Andersen, and N. Davidson, Phys. Rev. A **66**, 045401 (2002).

[42] J. Ringot, P. Szriftgiser, and J. C. Garreau, Phys. Rev. A **65**, 013403 (2002).

[43] W. Happer and B. S. Mathur, Phys. Rev. **163**, 12 (1967).

[44] D. Cho, J. Korean Phys. Soc. **30**, 373 (1997).

[45] D. Schrader, I. Dotsenko, M. Khudaverdyan, Y. Miroshnychenko, A. Rauschenbeutel, and D. Meschede, Phys. Rev. Lett. **93**, 150501 (2004).

[46] M. Kasevich and S. Chu, Phys. Rev. Lett. **69**, 1741 (1992).

[47] S. E. Hamann, D. L. Haycock, G. Klose, P. H. Pax, I. H. Deutsch, and P. S. Jessen, Phys. Rev. Lett. **80**, 4149 (1998).

[48] D.-J. Han, S. Wolf, S. Oliver, C. McCormick, M. T. DePue, and D. S. Weiss, Phys. Rev. Lett. **85**, 724 (2000).
[49] B. P. Masterson, C. Tanner, H. Patrick, and C. E. Wieman, Phys. Rev. A **47**, 2139 (1993).
[50] H. Häffner, S. Gulde, M. Riebe, G. Lancaster, C. Becher, J. Eschner, F. Schmidt-Kaler, and R. Blatt, Phys. Rev. Lett. **90**, 143602 (2003).
[51] J. Y. Kim and D. Cho, J. Korean Phys. Soc. **37**, 744 (2000).
[52] B. C. Young, F. C. Cruz, W. M. Itano, and J. C. Bergquist, Phys. Rev. Lett. **82**, 3799 (1999).
[53] J. Ye and J. L. Hall, Opt. Lett. **24**, 1838 (1999).
[54] D. J. Wineland, J. C. Bergquist, W. M. Itano, and R. E. Drullinger, Opt. Lett. **5**, 245 (1980).
[55] D. J. Wineland, W. M. Itano, and J. C. Bergquist, Opt. Lett. **12**, 389 (1987).
[56] Y. Miroshnychenko, D. Schrader, S. Kuhr, W. Alt, I. Dotsenko, M. Khudaverdyan, A. Rauschenbeutel, and D. Meschede, Opt. Express **11**, 3498 (2003).
[57] T. G. Walker and M. Saffman, J. Phys. B **38**, S309 (2005).
[58] I. I. Ryabtsev, D. B Tretyakov, and I. I. Beterov, J. Phys. B **38**, S421 (2005).
[59] M. S. Safronova, C. J. Williams, and C. W. Clark, Phys. Rev. A **67**, 040303(R) (2003).
[60] F. Gounand, J. de Physique **40**, 457 (1979).
[61] T. F. Gallagher, *Rydberg Atoms* (Cambridge University Press, Cambridge, England 1994).
[62] M. J. Seaton, Mon. Not. R. Astron. Soc. **118**, 504 (1958).
[63] M. Marinescu, H. R. Sadeghpour, and A. Dalgarno, Phys. Rev. A **49**, 982 (1994).